Budapest University of Technology and Economics
Faculty of Electrical Engineering and Informatics
Department of Measurement and Information Systems

András Kufcsák

Maximum likelihood based determination of the position of annihilations in PET detectors

TDK report

Supervisors
Dr. István Kollár
Dr. Emőke Lőrincz

Budapest, 2014

CONTENTS

1 INTRODUCTION

The rapid evolution of science and technology over the last decades has promoted the advancement of many aspects of life. One substantial area is medicine where the combined knowledge in several branches of science results in the continuous development of new medical methods and treatments, new medical systems and devices. The ability of gathering information on the health status of a patient represents a fundamental cornerstone of a great majority of medical treatments. This is essentially crucial when the examined area concerns internal biological entities and disorders which are not directly accessible. Several different imaging methods have been devised to overcome this issue, among them a remarkable technique is tomography.

Tomography is a non-invasive procedure, which means that using this technique it is possible to collect information of the inner structures of the body without breaking the skin, or entering body cavities. The basic principle of tomography is to create images of cross-sections of the examined object, by combining sensed radiation images taken in different directions. These images are then used to compose the required information with the aim of a mathematical reconstruction process.

The two most commonly used tomography techniques in medicine are computer tomography, or CT (more specifically X-ray CT), and magnetic resonance imaging, or MRI. In the case of CT the cross section images are generated with x-rays. The introduction of this type of tomograph dates back to the 1970s. MRI systems use strong magnetic fields at imaging, and detect radiofrequency waves emitted by the excited atoms of the body. The first working MRI scanner was created around the 1980s. Over the years several different variations of tomography have been developed based on the physical phenomena used in the creation of images. These are e.g. gamma-rays, electrons, ions, and other particles and waves, or even simultaneously integrated phenomena.

Positron emission tomography (PET) is a type of tomography where imaging is based on detection of gamma photons. In contrast to CT and MRI, where anatomical structures could be investigated, PET explores physiological activities measuring changes in metabolism. In order to improve diagnostics

the extracted information on metabolism could be aligned with structural information. Functional and structural imaging is combined in PET/CT and PET/MRI multimodal imaging systems.

PET devices have been efficiently used in several clinical areas, most essentially in clinical oncology, neurology and cardiology. Beside the emerging clinical applications, its use is also significant in the pre-clinical field, where pharmacological experiments are carried out on animals.

The use of PET scanners improves the quality of healthcare. Providing more and more detailed information on the health status of a patient assists in better and earlier diagnosis. As a result, it could improve treatment options and enable better rehabilitation chances; hence it forms an active research area. The SPADnet project is initiated to develop a new type of PET detector system, which improves imaging capabilities whilst having a lower production cost, achieves higher quality and wider spread of such devices. This is intended to be achieved through the development of detector modules supplied with CMOS-based light sensors. The Department of Atomic Physics of the Budapest University of Technology and Economics (in the Physical Institute of the Faculty of Natural Sciences) takes part in this research as a member of the project, among several European universities and research institutes.

A task in the operation of the detector module is to determine the planar position where gamma photons from the examined body impinge on the detector surface (point of interest, POI). During my involvement in the project at the Department of Atomic Physics I presented a method estimating this POI, based on a center of gravity (COG) algorithm. I also implemented this algorithm onto an FPGA connected to the sensor which has been implemented in the project. In this report I would like to investigate the performance of the maximum likelihood estimation (ML, MLE) of the POI, as a reference to qualify the performance of the COG method, and to see whether significant improvement is possible based using the very same sensor data. In theory, the ML method provides the "theoretically best" estimation. The report also tries to reveal the feasibility of an FPGA implementation of the ML method.

For this, first I introduce the basics and working principles of PET systems, the detector module and its parts, and I present the positioning task, its role and its properties. In the second section I describe the MLE method and its features; I introduce the model I used for the ML method, and review my

findings about positioning with MLE. Further subsections concern a direct comparison with the COG method, and considerations of a possible FPGA implementation. The final section of the report frames a summary with further considerations for future work in the topic.

2 PET SYSTEMS

2.1 BASICS OF PET

2.1.1 STRUCTURE AND WORKING PRINCIPLE

Positron emission tomography imaging of functional and physiological activities is implemented through the detection of spatial distribution of a certain tracer material injected into the body. This tracer is a chemical compound, in which radioactive isotopes are tightly bonded to biologically active molecules. In most of the cases the isotope carrier is a glucose molecule which is spread within the body with biochemical reactions. The radioactive decays indicate the path of the tracer and the regional glucose uptake. Measuring the concentration of the tracer through the detection of the decays is suitable for predicting and detecting mutations and diseases (e.g. weak cells take up less substance, while cancerous cells have a higher volume of metabolism). With this technique PET is capable of detecting areas in molecular detail. The used radioactive isotopes are short half-life isotopes with low radiation dose. The most often used types are carbon-11, nitrogen-13, oxygen-15, aluminum-26, fluorine-18 and rubidium-82. These are isotopes that undergo β^+ decay, which means a proton is converted into a neutron in these materials, while releasing a positron and a neutrino.

As the isotope undergoes a decay, it emits a positron. The positron is the antiparticle of the electron, it has the same mass as an electron, but has the opposite charge. The emitted positron has a high kinetic energy, but it decelerates and loses its energy as traveling in the body tissue. Depending on the applied isotope, it takes around a millimeter distance until the positron reaches an energy level low enough to react with low-energy electrons of the body tissue. When this low-energy electron positron pair collides, they undergo a physical reaction called annihilation. In the annihilation process the particles are transformed into new particles, while satisfying certain conservation laws, such as the conservation of electric charge, the conservation of linear momentum and total energy, and the conservation of angular momentum. The most probable case the conversation laws allow is that the electron-positron collision results in the creation of two gamma photons. As total energy is

conserved, the energy of the gamma photons equals the total energy of the positron-electron pair, the mass converted to energy, i.e. 511 keV for each gamma photon. As the collided particles are almost at rest before the annihilation, there is no linear momentum of the system at the reaction; hence the conservation of linear momentum results in the emission of gamma photons moving in opposite directions. (Annihilation could also occur with electrons and positrons having appreciable kinetic energies, this results in the creation of other heavy particles.)

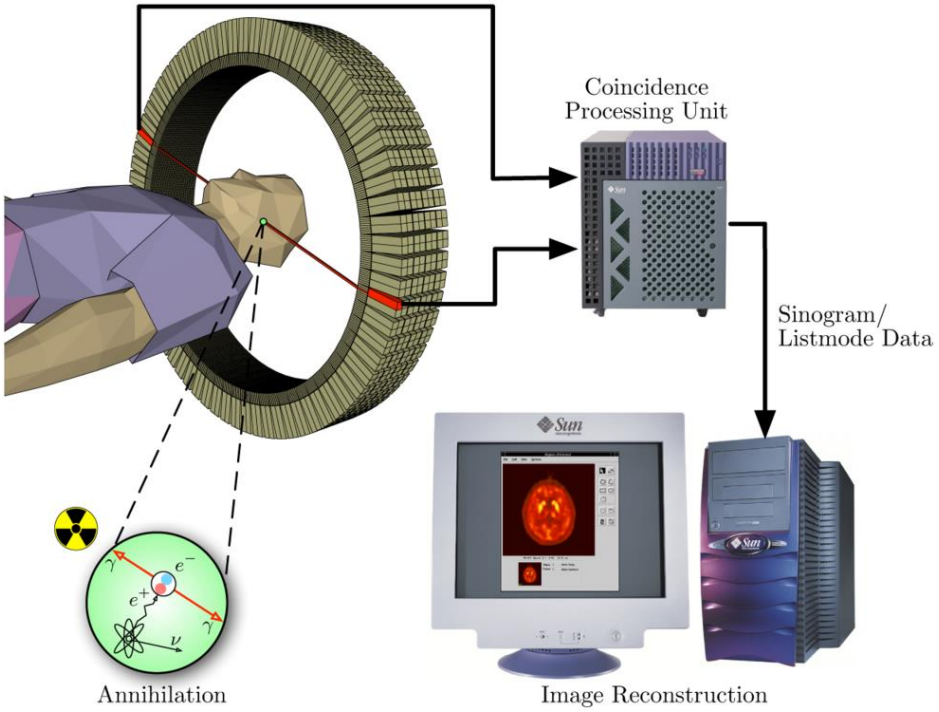

Figure 1. Working principles of PET (Wikipedia: Positron emission tomography)

The detection of these gamma photon pairs are used to gather information on the spatial distribution of the decaying tracer in the body. The gamma photons moving in opposite directions are detected with gamma photon detector modules built up in a circular arrangement. The detection of gamma photons on opposite sides of the detector ring could designate a line, on which the annihilation occurred, this is called the line of response (LOR). For this, gamma photon pairs from the same annihilations have to be detected. In order to achieve this, every single gamma photon detection is labelled with a timestamp, and only gamma photons on opposite sides of the ring which have almost the same time stamp are kept. The time frame for pairing gamma photons (coincidence

window) is usually 3-10 ns wide. The described working principle is depicted on Figure 1. Working principles of PET

2.1.2 IMAGE RECONSTRUCION

Using the LORs, two dimensional image slices (tomograms) could be generated in the plane of the detector ring. For this, the angle of a LOR is registered in function of its displacement from the center of the ring. Considering a certain point in the field of view (FOV), and registering all the LORs designated by gamma photons from this point results in shape of a sine wave (Figure 2. Using LORs to create sinograms). Accounting all the LORs in the plane of the ring could be considered as plotting projections along the direction of parallel LORs (Figure 3. The relation of projections and sinograms The plot of all projections in function of the angle of the parallel LORs is called a sinogram. Sinograms could be processed to gain 2D images with different image reconstruction processes, e. g. forward back projection (FBP), inverse radon transformation, ML-EM (maximum likelihood – expectation maximization), or OS-EM (ordered subsets EM). Different image reconstruction methods allow the tuning of complexity in contrast with accuracy. 3D images are built up either using a set of 2D images, or applying more than one detector ring, and allow coincidence detection between different rings.

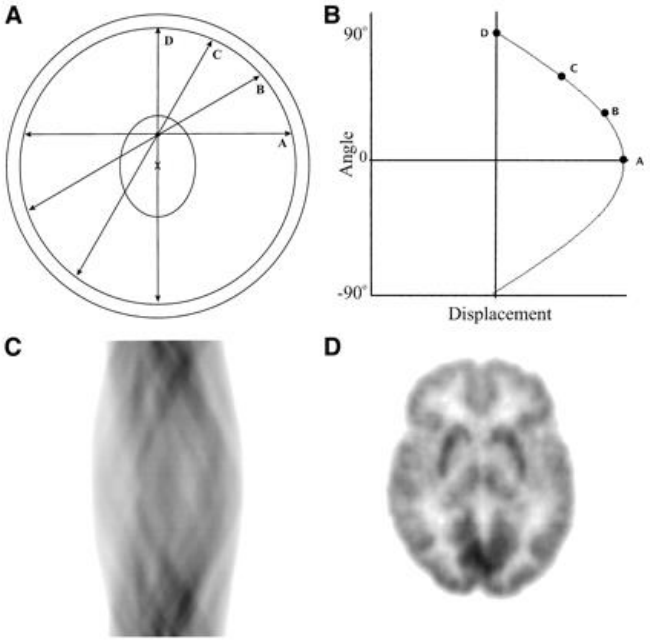

Figure 2. Using LORs to create sinograms (Frederic H. Fahey, 1. June 2002)

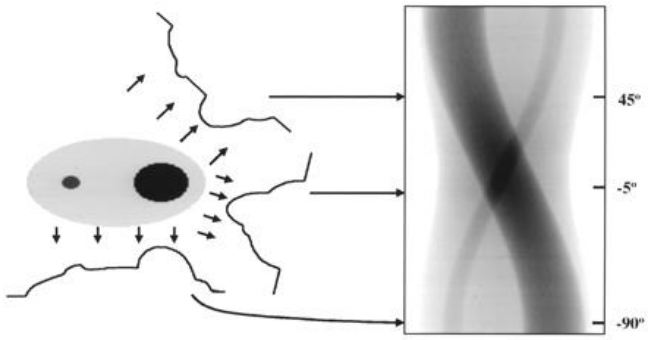

Figure 3. The relation of projections and sinograms (Frederic H. Fahey, 1. June 2002)

The above described method has however several limitations on the resulting resolution of the FOV. First of all, even if the position estimation of the annihilation was perfect, it still would differ from the position of the decays of the tracer, since positrons could travel up to a few millimeters from the point of emission before colliding with an electron. This distance is dependent on the applied tracer, and the electron density of the examined tissue, and it is usually corrected in the reconstruction algorithm by applying a localization dependent blurring on the intensity function describing the density of decays. Secondly, as the colliding particles at annihilation often possess kinetic energy, the

resultant momentum of the emitted gamma photons will differ from zero as well, which means, that the direction of their movement won't be collinear. This phenomenon is called non-collinearity or acollinearity, and causes a resolution loss in the FOV (Figure 4. Acollinearity). For detector rings of larger diameter the loss in resolution is higher accordingly.

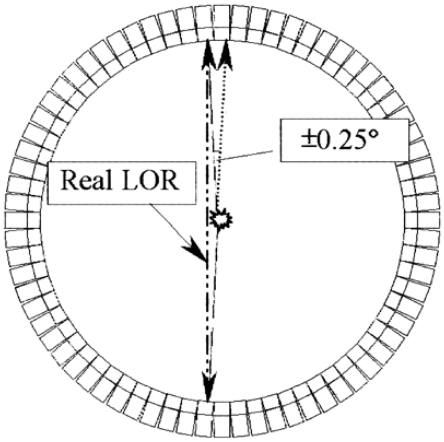

Figure 4. Acollinearity (Tarantola, Zito, & Gerundini, 2002)

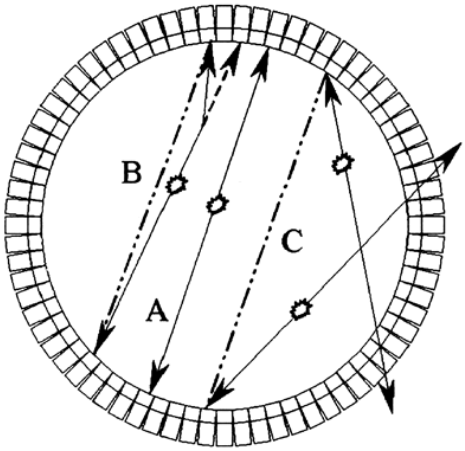

Figure 5. Coincidence types: true coincidence (A), scattered coincidence (B), random coincidence (C) (Tarantola, Zito, & Gerundini, 2002)

Another noise factor is the recording of gamma photon coincidence pairs, which are originated from different annihilations, but have a timestamp difference smaller than the coincidence window. These are called random coincidences, and designate LORs which do not account for real decays (Figure 5.

Coincidence types: true coincidence (A), scattered coincidence (B), random coincidence (C)). The noise caused by random coincidences could be somewhat reduced with a robust reconstruction algorithm. Sometimes gamma photons of an annihilation scatter on the particles of the tissue. The phenomena of Compton scattering, is that a photon reacts with a charged particle. In the inelastic collision of the particles the trajectory of the photon deviates, while the photon loses energy. This way the original gamma photon pair still impinge on the detector, but the assignment of the LOR will be incorrect. As the energy of the gamma photons decreases during scattering, a simple way to filter these events out could be applying an energy threshold on the detected photons.

2.2 THE DETECTOR MODULE

It is described, that the recording of LORs requires the detection of gamma photons from the annihilations with detector modules of the detector ring. The basic concept of this detection is that a gamma photon is absorbed in a so called scintillator crystal. The scintillator crystal is a material which absorbs the energy of an incident radiation and re-emits this energy in the form of light (photons). The produced light is sensed with a light sensor attached to the crystal, and turned to electric signals. We expect the detector to suit several requirements. To reduce the radiation dose on the patient, only a limited amount of tracer could be injected into the body. In order to gather a sufficiently large amount of information, it is important, that a large number of annihilations are accounted. This means, that the detector has to be sensitive, i.e. it should absorb all gamma photons of 511 keV in the plane of the ring. Beside it has to have a good energy resolution, so it would be possible, to filter out events with a different energy level. With this, scattered gamma photons, and noise of the crystal can be omitted.

The position of the gamma photon absorption in the crystal has to be determined using the output signals of the light sensor. This is important for better recording of LORs, hence the resolution of the gamma position estimation affects the resultant resolution of the FOV. This way, a good resolution of position estimation is desirable. In order to correct parallax error (a certain limitation factor of the detector module which is described later), it is useful to estimate not only two dimensional position of the gamma photon impingement (point of interest, POI), but the depth of this position (depth of interest, DOI) as well.

The detector also has to have a good timing parameter, for effective coincidence measurement. The time between excitation and relaxation of the scintillator crystal depends on its material. Using detectors with a resolving time of a few hundred picoseconds, it is possible to assign the position of the annihilation to a smaller region on the LOR. This is called time-of-flight (TOF) technique, and it is based on measuring the time difference between impingements of the two gamma photons of an annihilation. A higher timing resolution thus leads to improved signal-to-noise-ratio (SNR) of the image, which means the capability of achieving the same quality of image using fewer events (lower radiation).

Another essential parameter is the constructional cost of a detector module. The above stated (often contradictory) requirements of the detector require deep considerations which lead to the usage of a number of different scintillators, light sensors, and detector constructions.

2.2.1 SCINTILLATOR CRYSTALS

The most essential parameters of a scintillator crystal are the following. Density, stopping power and absorption length, luminosity or light yield, energy resolution, background radiation, decay time (fall time and rise time), emission spectrum and emission peak, refractive index, other mechanical properties and cost. Density is measured in g/cm^3, and is dependent on the material of the crystal. Stopping power expresses the efficiency of “stopping”, absorbing the incident particles. It is defined as the retarding force acting on the particle when interacting with the crystal material while losing energy. If density and the atomic number of the crystal material are higher the better is stopping power. Higher stopping power results in shorter absorption length, which is the length on which probability of not absorbing a particle drops to 1/e fraction of its initial value. This is also called attenuation length.

Luminosity or light yield is expressed as photons/MeV which tells the number of generated light photons per unit of energy of the incident particle. In order for the detector has a good SNR and energy resolution, a higher light yield of the scintillator is desirable. This means, that the number of generated light photons is dependent on the crystal material and energy of the incident particle. On average this counts from few hundred to a few ten thousand photons.

Energy resolution expresses the widening of the photopeak. If we plot the count rate of absorptions in function of the absorbed energy, we get the energy spectrum of the scintillator (Figure 6. Typical γ–energy resolution curve of a scintillator). The photopeak is the part of the energy spectrum, which is due to complete absorptions of gamma photons. To put it in a simple way, energy resolution represents the ability of distinguish between real gamma photon absorptions and other events (scattering in the crystal, background radiation, noise). Energy resolution is often expressed as a ratio of the "full-width-at-half-maximum" (FWHM) of the photopeak to the peak position.

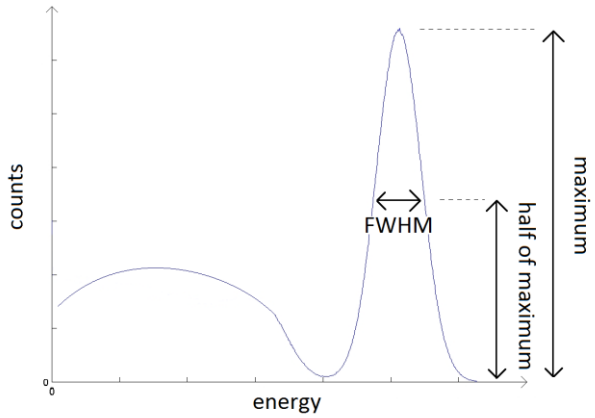

Figure 6. Typical γ–energy resolution curve of a scintillator

It is already mentioned that for coincidence measurements a scintillator of good timing resolution is needed, especially for TOF PET systems. Rise time is defined as the time interval during the light pulse amplitude rises from 10% to 90% of its maximum. The pulse falls exponentially, fall time is the time interval that 1/e fraction of the energy of the pulse is emitted after.

It is important from the aspect of the light sensor, that it shall be sensitive to the spectral range of the emitted light. Certainly, the scintillator has to be transparent to its own scintillation light as well. The peak of the emission spectrum is expressed in nanometers, as a parameter of the scintillator. The detector construction often includes optical coupling, thus the refractive index of the crystal could be essential too. Other mechanical parameters play an important role, since they highly affect production and mechanical shaping possibilities and costs. To meet the above stated requirements,

current applications and experiments usually apply scintillator materials of NaI(Tl), BaF2, BGO, LSO, GSO, LYSO, LaBr3, LFS, LuAP, and LuI3 compounds.

2.2.2 LIGHT SENSORS

2.2.2.1 PHOTOMULTIPLIER TUBES

Originally the detector consists of a scintillator crystal coupled to a photomultiplier tube (PMT) (Figure 7. Photomultiplier tube . Light photons of the scintillation strike the photocathode of the PMT, where electrons are generated through the photoelectric effect. Then a focusing electrode directs these primary electrons towards the dynodes of the PMT. The dynodes are held at increasingly higher voltages. This way the electrons are accelerating by the electric field moving towards the next dynode. When the accelerated electrons hit the dynode more electrons are generated through the process of secondary emission. The large number of electrons hitting the anode could cause a current pulse which is easy to detect.

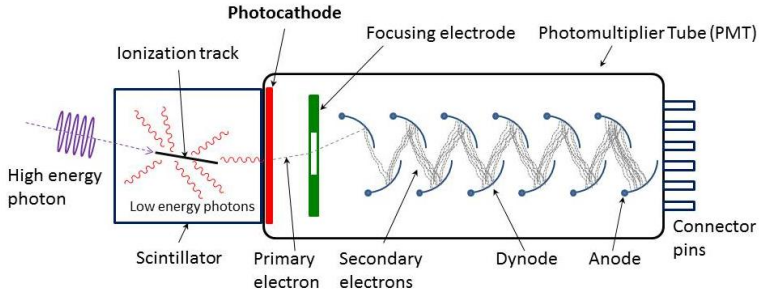

Figure 7. Photomultiplier tube (Wikipedia: Photomultiplier)

In order to achieve a better spatial resolution of the detector, scintillator crystals are cut to small sizes in a cuboid shape and arranged in an array configuration. Crystal arrays today contain up to a few hundred (or even a thousand) crystal pins, and have a pitch of a few millimeters. This small size of a crystal pin does not allow the coupling of PMT tubes of bigger size directly to each pin. Attaching PMTs to each crystal is not only impossible because of the size of PMTs, but the resulting number of electronic channels and PMTs and its cost. Thus, an array of less number of PMTs is attached to the crystal array. A thin light guiding glass is placed between the sensors and the crystals, which allows

the scintillation light of the yielding crystal pin to reach several PMTs (Figure 8. Detector with crystal array). The position of the yielding crystal is then determined calculating the center of gravity of the PMT signals. This technique will be described more detailed in a later subsection.

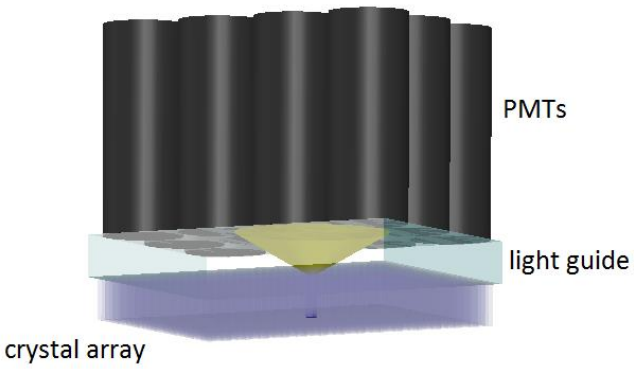

Figure 8. Detector with crystal array (Steinbach, 2011)

Improving the detector performance, research and development has been being carried out in the field of light sensors along scintillator crystals and detector constructions. PMT manufacturing companies started to construct multi-channel PMTs. These PMTs contain 4-256 channels working as independent photomultipliers, assembled to a common package. This way the big size of PMT arrays of individual packages can be eliminated, and the dead space between sensitive surfaces could be reduced. Channels could be worked up several ways depending on the types of dynodes for different photometric purposes (Figure 9. Dynode structures in PMTs).

Mesh type dynodes are meshed electrodes which are placed close together. The most essential benefit of these devices is the excellent output linearity.

Metal channel dynode structures consist of extremely thin electrodes. These electrodes are fabricated with advanced micromachining techniques. Stacking of the electrodes is done very precisely using simulations of electron trajectories. Their benefits are excellent timing performance (because of the close proximity of electrodes, and the resulting short path of electrons), stable gain, low crosstalk and compactness.

A different dynode structure is microchannel plate (MCP). This is a very thin (around 1 mm) disc consisting of micro glass tubes (capillaries) parallel to each other. The number of the glass tubes

could take up to a million, and each of them acts an independent electron multiplier. A result of this structure is an outstanding timing, the device also has high gain despite its compact size. MCP PMTs are available with one anode as output, or with multiple anodes, in this case the device is capable of two dimensional detection.

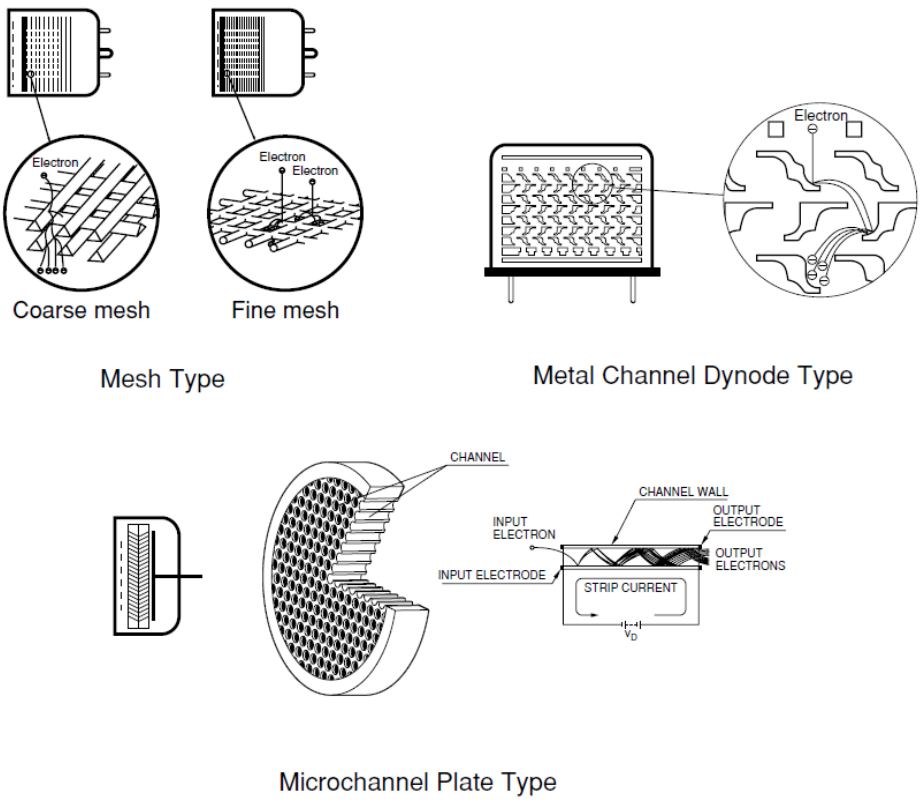

Figure 9. Dynode structures in PMTs (Hamatsu, 2006)

There are dynode structures existing combining the above mentioned and different dynode structures.

The channels of a multi-channel PMTs could either have a matrix type, or a linear type arrangement. These devices have a position sensitive capability. Depending on the method for reading out the output signal of a position sensitive PMT, two major categories could be distinguished. A multi anode PMT has a number of outputs proportional to the number of channels (Figure 10. Different anode structures of a PMT with metal channel dynodes). The number of output anodes however could be

decreased, using cross-plate or cross-wire anodes, which applies a center-of-gravity detection using a charge-division readout circuit. In these tubes the secondary electrons are reflected back from the last dynode and read out by cross plate anodes which are arranged in two layers, intersecting with each other (Figure 10. Different anode structures of a PMT with metal channel dynodes). This way a cloud of charges in the PMT tube is sampled on the anode wires in a ratio, which is dependent on the point of the gamma interaction. These devices are called position-sensitive photomultipliers (PSPMT). The method to gather position information using the anode wires is described in a later subsection.

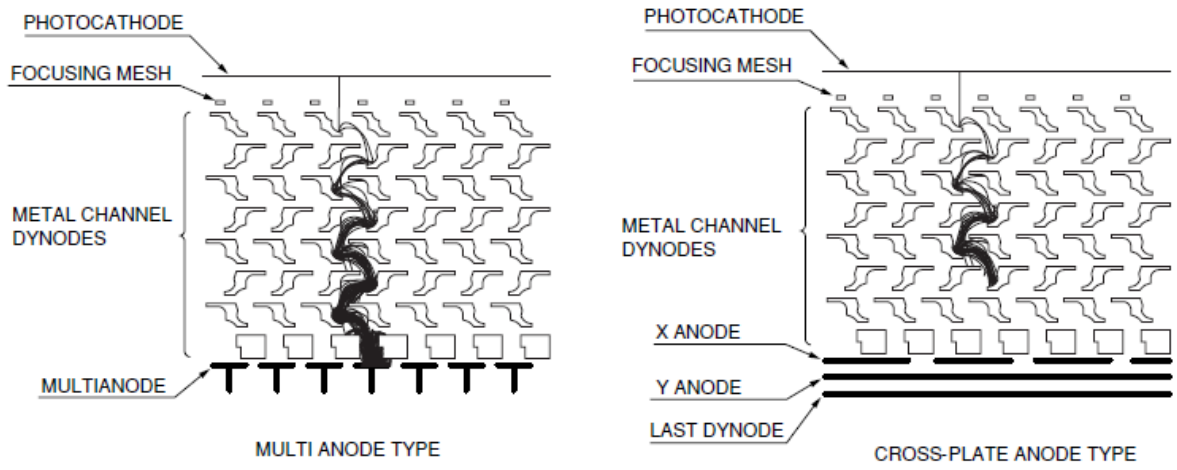

Figure 10. Different anode structures of a PMT with metal channel dynodes (Hamatsu, 2006)

PMTs in compact cases as modules are often incorporate additional circuits as high-voltage power supply, voltage divider circuit for the dynodes, other operating circuits (gate circuits, photon counting circuits), interface to PC, cooling device, even optical appliances (e.g. mirrors, band-pass filters). The available varieties of PMTs differ in several other viewpoints such as materials used in the device (for the photocathode, window, etc.), quantum efficiency (number of emitted photoelectrons per incident photons), luminous sensitivity, uniformity (variation of the output with respect to the position where light photon is scanned on the cathode), gain, SNR, speed, stability (output variation), housing, etc. which affects their efficiency and usability in different applications.

2.2.2.2 SOLID STATE LIGHT SENSORS

Along the evolution of detector modules, solid state light sensors are also started to be under investigation. Main advantages of these devices, that they could be manufactured in an extremely small size, and that they are insensitive to electromagnetic fields. The small size enables one to one coupling of scintillator crystals and light sensors, which increases spatial resolution of the detector, and provides high compactness when used in an array. Insensitivity to electromagnetic fields permits the development of hybrid PET/MRI systems, resulting in a more efficient diagnostic in contrast to PET/CT systems. Another advantage of solid state light sensors is the low operation voltage, which eliminates high voltage power supplies, and voltage divider circuits used with PMTs. Furthermore, solid state devices could be manufactured in high volume, with relative low cost.

The basic solid state construction for light detection is the PIN diode. PIN diodes are reverse biased when used to light detection. Normally, if a photon of sufficiently large energy enters the depletion region of a reverse biased diode, it creates an electron-hole pair. These charge carriers are swept out from the depletion region without recombination, producing a current. In PIN diodes there is a lightly doped, wide intrinsic region between the p-type and the n-type regions, which extends the depletion region. The wider depletion region is responsible for increasing quantum efficiency (percentage of photons producing charge carriers to those hitting the sensitive area of the device). However a photocarrier generation even could occur in dark, due to thermally generated carriers and background radiation, this is called dark current. Other drawbacks of this type of device are that the low photo-current requires amplification with very low noise amplifiers, and the fact, that the usage of wider intrinsic regions for higher quantum efficiency results longer paths for charge carriers, which decreases the speed of operation.

Avalanche photodiodes (APD) overcome the low photo-current of PIN diodes. Applying a reverse bias voltage close to the breakdown voltage causes a high electric field in the depletion region. This field accelerates carriers until they reach a kinetic energy high enough to create electron-hole pairs when colliding with bound electrons. This process is called impact ionization. If the generated electron-hole pairs produce more pairs, an avalanche breakdown occurs producing a breakdown current. This way the device has a built-in gain, depending on the applied voltage. The multiplication factor of the device moves around 10^2-10^3, depending on manufacturing techniques (doping and beveling). Unfortunately avalanche breakdowns also amplify the dark current. Another difficulty in the

application of APDs, is that the gain densely depends on temperature, which requires further electronics to stabilize.

With single photon avalanche diodes (SPAD) an even higher multiplication factor is achieved, using a voltage which is higher than the breakdown voltage. This case the electric field is so high (above $3x10^5$ V/cm), that even a single photon could result an output current in milliampere range with picosecond timing. This kind of operation is called Geiger mode, hence devices manufactured to target this mode are also called Geiger-mode APDs (G-APD). For the sake of protection of the device, the output current has to be quenched immediately after breakdowns. This either could be done in a passive or in an active way. In passive quenching a high ballast load resistor is connected serially to the SPAD. As breakdown current causes a voltage drop on the load resistor, it decreases the bias voltage of the diode, which suppresses the current. As the voltage drop decreases with the decreasing current, the bias voltage recovers up to its initial value enabling the diode to sense again. In active quenching a specific circuit detects the onset of the breakdown current, and triggers a digital output. It quickly reduces the bias voltage below breakdown voltage to quench the current then increase the bias again to enable further detections. An important parameter of the device is the time it spends with recovery, since no detection could be carried out during that time (dead time). Above a certain light intensity breakdowns occur so frequently, that the device is not capable of proper detection because of the dead time, the detector saturates, and the output won't be proportional to the real light intensity. This is furthermore harmful for the device, because of the almost continuous breakdown current. SPADs are also sensitive to thermal generated and background radiation caused breakdowns (dark count), the noise of the device can be described with the number of dark counts per second (dark count rate, DCR). For a proper operation it is expected, that a sufficiently long time passes between breakdowns (desirably a few milliseconds).

The latest and most promising solid state photodetectors are silicon photomultipliers (SiPM). These devices consist of an array of SPADs on a common substrate. Analogue SiPMs use passive quenching technique on the SPADs. Each SPAD provides a trigger output marking the detection of a photon realizing a switching mode. As SPADS are connected parallel, the almost simultaneous breakdown in two or more SPADS would result a stepped output. However, on-chip capacitances and inductances blur this output resulting in an analogue output in a dynamic range. If photon count or other detailed

information is needed to be extracted from this signal, complex application specific circuits (ASIC) have to be used.

Digital SiPMs apply active quenching technique including a 1 bit A/D per SPAD and provide fast restoration and shorter dead time. Using A/D conversion per SPAD output (1bit) (instead of on the resulting output signal) highly increases SNR. Digital SiPMs are suitable for the utilization of on-chip logic beside the sensitive area. This includes summation of the digital signals for photon counting. Photon detection is also accompanied with time measurement of ten picosecond resolution. Digital timestamps are provided through the use of ring oscillators and asynchronous counters, which provide timing information in digital values (time to digital converter, TDC). A further option that SPADS could be switched off individually, preventing noise from noisy and faulty SPADs. The digital concept enables many further possibilities, additional logic could be employed for signal processing, error correction or other functions realizing a system-on-a-chip (SOC) design.

SiPMs usually include a few times hundred up to a thousand pixels per square millimeter. Their gain is about the same as for PMTs (10^5-10^6), but they outperform conventional PMTs in several aspects. The applied voltage of 20-80 V is only a fraction than for PMTs (over a thousand volts), they have higher quantum efficiency (around 80%), and better timing properties than most PMTs (10-100 ps). SiPMs have features of compact packaging and relatively low production cost. The construction of SiPMs has its own challenges too, however. Additional logic on the substrate is present as dead space in sensation, which deteriorates the fill factor (proportion of sensitive area to the whole surface). There is an inevitable area between SPADs as well to reduce optical cross talk, which increases dead space. This could be improved by applying SPADs with bigger sensitive areas, but in turn this increases the dark count rate, more than linearly with SPAD size. To fulfill both requirements requires deep considerations and complex planning. Another drawback of these devices is that the number of electronic channels with many SPADs is difficult to handle.

The utilization of solid state technology also appeared in PMTs. Hybrid Photo-Detectors (HPD) are photomultiplier tubes applying semiconductor devices. This device consists of a photocathode, which emits photoelectrons towards an APD, where the number of photoelectrons is increased. It provides extremely good pulse height resolution, very small gain variation, and little multiplication fluctuation.

2.2.3 DETECTOR CONSTRUCTIONS

As described earlier, the very first PET detectors consisted of individual scintillator crystals applied to a photomultiplier tube. Detectors which have been used at most PET systems in the last decades are based on the detector block, introduced in 1986 (Casey & Nutt, 1986). These devices consist of an array of scintillator crystals attached to an array of PMTs. The array of crystals could be formed from a relatively large scintillator material which is segmented to an array of smaller crystal elements using saw cuts (Figure 11. Detector block of four PMTs and segmented block crystal, Figure 12. Detector using segmented crystal). Filling the cuts with reflective materials, crystal segments could be isolated. The depth of the cuts could be used to adjust the sharing of scintillation light between PMTs, with respect to the interaction position of the gamma photon. By carefully designing the depth of the cuts, scintillation light will be unique for each element of the crystal as interaction position, thus, it is easier to assign the estimated gamma position calculated from the PMT outputs to the yielding crystal element (this is described in the next subsection).

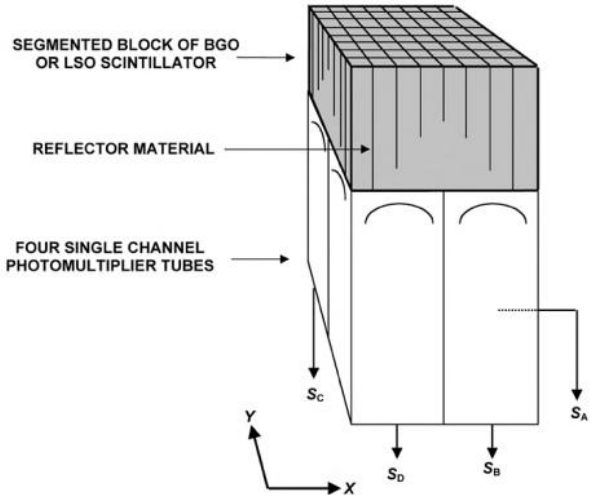

Figure 11. Detector block of four PMTs and segmented block crystal (Phelps, Cherry, & Dahlbom, 2006)

The crystal array could be built up from small crystal pins as well, attached to each other. The crystal pins of the array are isolated having a reflective surface. The array is coupled to the light sensor array using a light guide (Figure 8. Detector with crystal array). This sort of detector design was improved

by utilizing PSPMT sensors for scintillation light detection. The better spatial resolution of these devices allowed the distinction of yielding crystals using the PSPMT output, even with small crystal sizes. Applying solid state detectors such as APD arrays or SiPMs with a scintillator array further improves this technique, enabling even smaller crystal sizes. Smaller crystal pins are desirable, since gamma position is assigned to a yielding crystal element, thus the resolution of position estimation is limited by the crystal pitch. The pitch of the crystals today could be low as around 1 mm (or even down to 0.5 mm). With this size, the arrays include up to a thousand pins.

It is said earlier, that the size of solid state light sensors (PIN diode, APD, SPAD) allows one to one coupling of crystals and light sensors. This sort of approach however has not spread, as manufacturing crystal pins below a certain size is technologically elaborate and the proportion of sensitive area decreases on the surface of the crystal array, because of the insulation between crystals. Nevertheless, the perfect alignment requires unsubstantiated efforts which do not make this type of design rewarding. Instead another type of detector is utilized, using crystal slabs (Figure 13. Detector using crystal slab). In the case of crystal slabs or often noted as continuous crystals, a larger thick piece of scintillation crystal is attached to a light sensor (PMT array, PSPMT, APD array, or a SiPM) with a light guide between. This approach is called Anger camera or gamma camera. The resolution of the detector module in this case is not limited by the pitch of crystal pins, but raise several requirements towards the parameters of an applicable scintillator material, and complex algorithms for gamma photon position estimation.

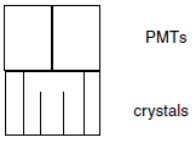

Figure 12. Detector using segmented crystal (Lewellen, 2008)

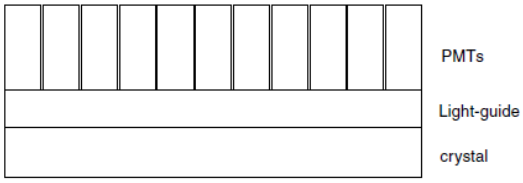

Figure 13. Detector using crystal slab (Lewellen, 2008)

Beside conventional detector constructions it is worth to mention that other approaches are continuously being under investigation. Most of these methods have been explored in order to extract DOI information as well (Lewellen, 2008; Peng & Levin, 2010). One method to gather discrete DOI is pulse shape discrimination (PSD). In this approach different types of scintillators are attached on the top of each other. Different type could mean different scintillator material, different shaping of crystal pins, or simply an offset in position of the second layer to the first. As different timing parameters of the different scintillators causes differing signal shapes on the light sensors, processing these signals are used to assign the crystal, in which the gamma photon is absorbed. (This is also called phoswitch design). This way the theoretical DOI resolution depends on the length of different scintillators, however light loss in the crystals and variation of timing parameters decrease this theoretical resolution. Manufacturing costs of these complicated structures also represent a crucial drawback, while complex processing units are required for signal processing.

Another technique for discrete DOI information is when complete detectors of short crystals with light sensors are stacked on each other. There are several different arrangements and approaches for this technique. The attendant of this method is an increasing number of channels/outputs, and increasing costs.

Continuous DOI can be extracted using light sensors on both end of the scintillator, and calculating time differences in detection of photons from the same absorption.

Another type of detector is the semiconductor strip detector (Bassignanaa, et al., 2012).These are crystal slabs which have parallel anode and parallel cathode strips on opposite sides of the slabs, but anode and cathode strips run in a perpendicular direction (Figure 14. Semiconductor strip detector). Applying a high potential difference on the anode and cathode strips, photogenerated carrier pairs drift towards the strips inside the crystal. The density of strips impacts the two dimensional position

of the gamma photon, difference of time in detection on the sides is used to estimate DOI. The device has a 3 dimensional spatial resolution of around 1 mm. The materials most used in these devices are cadmium-zinc-telluride (CZT), cadmium-telluride (CdTe), high purity germanium (HPGe). These detectors usually have poor timing properties because of low charge mobility.

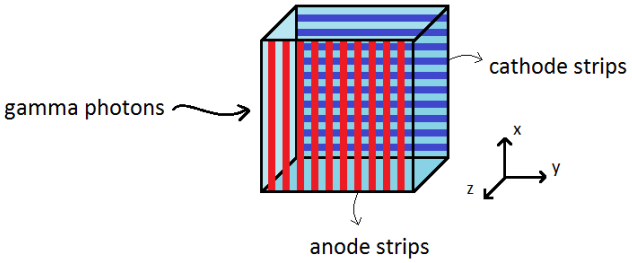

Figure 14. Semiconductor strip detector

The above described detectors and methods are not described more detailed in this report.

2.2.4 POSITIONING

Positioning means the task of finding the position of gamma photon absorption in the scintillation crystal using the output of the light sensor. This either could mean a 2 dimensional position, or a three dimensional position with depth information. It makes no sense to talk about positioning in the case of single crystals attached to individual PMTs. In the case of block detectors, in early PET systems positioning was carried out applying hardware solutions exclusively. This method is based on a COG calculation of the PMT signals. Taking into consideration a crystal array viewed by four PMTs in a rectangular arrangement (Figure 15. PMT signals for COG calculation), the ratio of PMT signals are calculated to gain the estimated 2 dimensional position in the following way:

$$X = \frac{B+D}{E} \tag{1}$$

$$Y = \frac{A+C}{E} \tag{2}$$

$$E = A+B+C+D \tag{3}$$

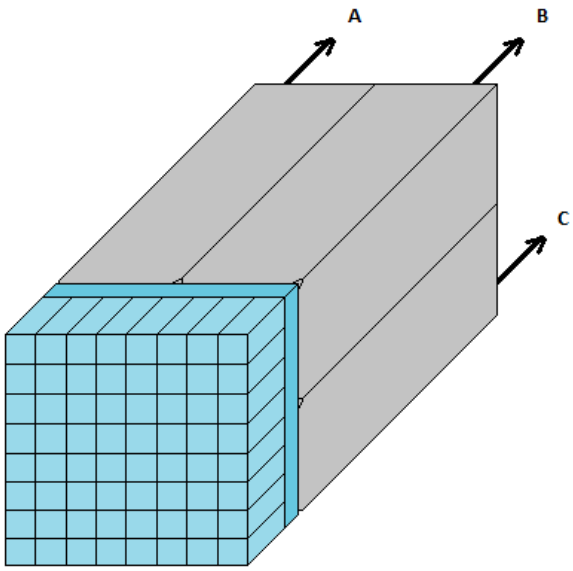

Figure 15. PMT signals for COG calculation

This approach is still being utilized, but each system differs in the details, forming a great variety of positioning methods. If the PMT array consists of several PMTs, a resistive (or capacitive) charge division circuit is used to form 4 corner signals, which can be used to estimate the position in the same center-of-gravity manner (Figure 16. An example for resistive charge division circuits). This is a very simple solution which only requires a few number of channels, however the noise of the charge divider circuit increases overall system noise.

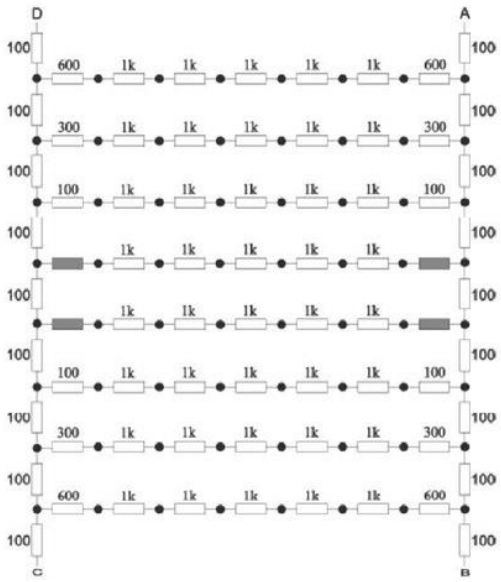

Figure 16. An example for resistive charge division circuits (A 2D Positioning Application in PET Using ANNs (Artificial Intelligence))

We have seen, that the number of anodes is decreased in PSPMTs. E.g. for a PSPMT of 16x16 channels, the number of cross-wire (output) anodes is 6 (on X axis) + 6 (on Y axis). Cross wire anodes are read out using a same type of charge division circuit used for multichannel PMTs, creating the four signals which could be used for COG positioning (except that charge is divided on a line of resistors in this case, not in a net of resistors) (Figure 17. Charge division circuit for PSPMTs).

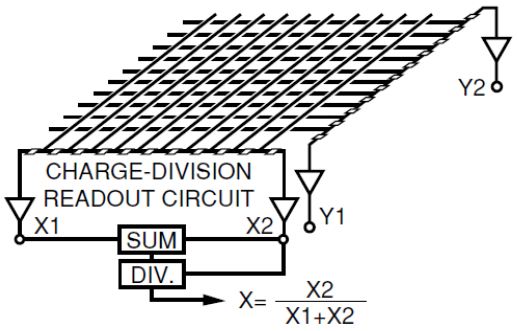

Figure 17. Charge division circuit for PSPMTs (Hamatsu, 2006)

As described earlier, in the case of crystal arrays, position of the gamma interaction is assigned to the yielding crystal. However, the fact that light does not reach the detector surface uniformly when the POI is on the edge of the surface (namely, the detector edge cuts the light distribution) the COG will

not be accurate. If several gamma interactions are measured in each crystal of an array, one could gather a flood map clearly showing the distortion of estimated POIs over the surface (Figure 18. Example for flood map (LYSO crystal array of 8x8 pins attached to position sensitive APD). This is often plotted for one axis (Figure 19. An example for cross section of irradiation flood map (8x8 crystal pins, different scintillator materials)).

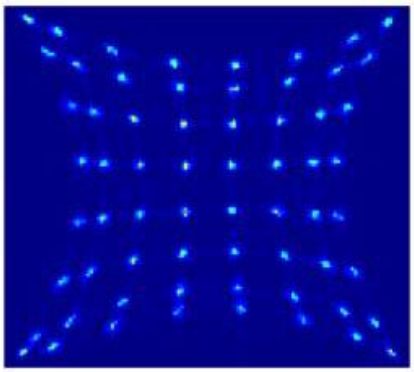

Figure 18. Example for flood map (LYSO crystal array of 8x8 pins attached to position sensitive APD) (Peng & Levin, 2010)

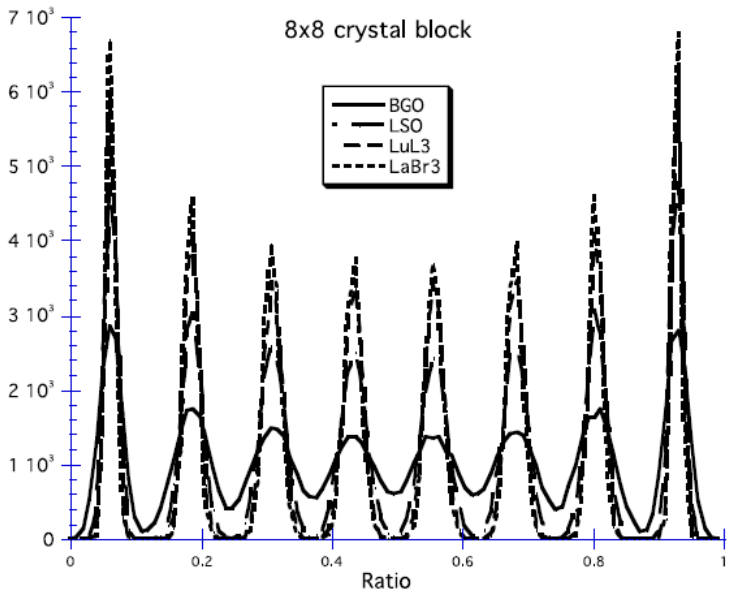

Figure 19. An example for cross section of irradiation flood map (8x8 crystal pins, different scintillator materials) (Lewellen, 2008)

The distortion is not only present because of the edge effect, but other uncertainties could deteriorate the accurate position estimation (variance in light sensor parameters e.g. anode gain non-uniformity, noise, etc.). Thus in order to decode which the yielding crystal is, a mapping of the calculated COG to the crystals has to be done, which could be considered as segmenting the flood map to regions of each crystal. This method is called segmentation, and the easier to separate the certain regions (not overlapping areas), the easier it is to carry out. (Figure 20. An example for segmentation (8x8 crystal array viewed by four PMTs)) It has been seen, that one way to improve this is to guide the light in a certain way to the light detector using saw cut crystals (Figure 12. Detector using segmented crystal). After all, the ability to decode the yielding crystal (the achievable resolution) depends on several properties of the detector.

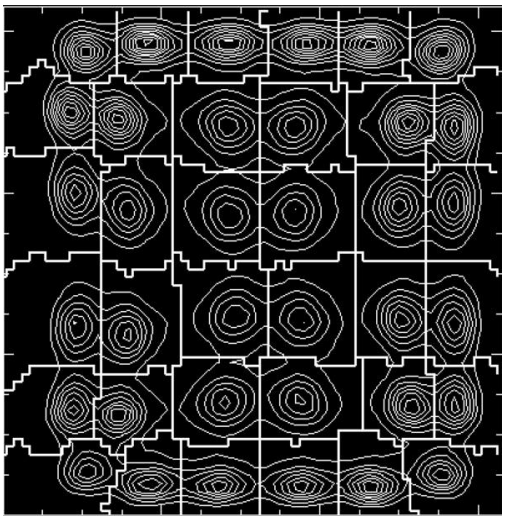

Figure 20. An example for segmentation (8x8 crystal array viewed by four PMTs) (Lewellen, 2008)

Later, hardware based positioning was supplied with software aid. This enables more sophisticated and more complex methods for error correction, and easement of processing. In certain systems, corrections are carried out directly on hardware level, improving detector properties (Popov, 2011). Software based positioning could either be carried out on a PC, or using a processing unit connected to the detector, even in real time (Kroeger, et al., 1997). Different systems have a great variety depending on the stage and where amplification, pulse shaping, and A/D conversion is done (Trotta, et al., 2008). Performance of the charge divider method is improved, by first amplifying and shaping PMT signals, then using the charge divider circuit (Pani, et al., 2004). Anode signals could be directly

amplified with a low noise amplifier and after sampling a software based positioning could be performed (Truman, Bird, Ramsden, & He, 1994; Trotta, Massari, Palermo, Scopinaro, & Soluri, 2007; Bird, Ramsden, & He, 1994). This way the charge divider circuit could be eliminated, but this technique requires further electronics, and employs several channels.

Resistive chains are also used with other type of light sensors, like APD arrays, MCPs (Fontbonne, 2013), or strip detectors. (Ishii, et al., 2011) Position sensitive APDs usually applies the same technique built in, and providing only the four corner signals.

The achievable resolution is dependent on the applied technique and differs heavily, but on average it is in the order of 1 mm.

The same COG method of four corner signals could be used with continuous crystal slabs as well, however the distortion of the light spread is still present. In this case the POI is continuous, hence no segmentation algorithm can be applied. Usually complex software based algorithms are needed to overcome this issue. Digital SiPMs have their benefit of providing digital data of small pixels. This way more information could be gathered from a scintillation, which is then used for a better positioning. As a trend, statistic based positioning methods are investigated for an accurate positioning. (Ling, Lewellen, & Miyaoka, 2007; van Dam, et al., 2011; Joung, Miyaoka, & Lewellen, 2002). These methods however incorporate high computational complexity. The desired resolution in case of these software based techniques is subpixel resolution.

2.2.5 LIMITATIONS

Beside certain limiting factors which have already been mentioned at the description of the applied devices (e. g. uncertainty of parameters of light sensor, scintillator properties), there are other limitation factors arisen at the detector level. Gamma photons penetrating the detector from an oblique angle designate an uncertain LOR. This is because most systems assume that gamma absorptions occur in a certain distance from the detector surface. In case if the real absorption occurred deeper in the crystal, the end point of the real LOR will be different. (This is irrelevant if gamma photons penetrate the detector from a perpendicular direction.) As a result, the FOV resolution will be lower closer to the ring, while having a better resolution in the middle of the ring.

This is called parallax error, and it is more significant with lower ring diameters and long crystal pins (Figure 21. Parallax error). As mentioned earlier estimating a DOI could correct this error.

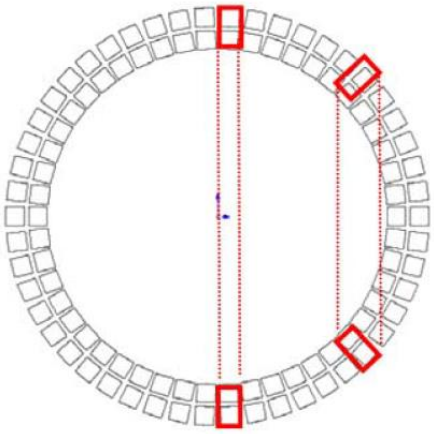

Figure 21. Parallax error (Peng, Olcott, Pratx, Foudray, Chinn, & Levin, 2007)

Another problem is the scattering of gamma photons inside the crystal. For most scintillator materials the probability of total absorption of the photon for the first interaction is below 50 %. This means, that a relative high number of incident gamma photons changes direction until a total absorption while producing light photons at each interactions. In case of a scintillator array, this means more than one yielding crystal which makes it harder to decode the crystals. A result of the relative low light output of a crystal the light distribution is affected by statistical uncertainties. In crystal arrays this leads to further misidentification of the crystal pins, which deteriorates spatial resolution. These limiting factors are depicted on Figure 22. Limitation factors in crystal arrays

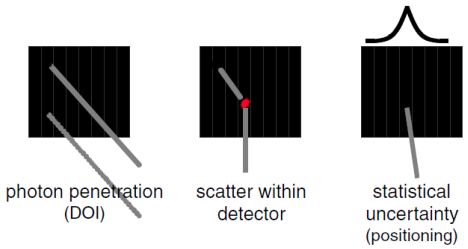

Figure 22. Limitation factors in crystal arrays (Lewellen, 2008)

In the case of a continuous crystal slab, we can think of the light generation in function of the position of gamma absorption as the light response function (LRF) of the crystal slab (basically, the spatial distribution of light over the sensor). This LRF is dependent on the DOI, which enables the calculation of DOI in Anger-cameras, however makes it more difficult to tell the 2D position of the incident gamma photon. Continuous crystal slabs often have retroreflectors on the side where gamma photons penetrate from, for better light collection, and as a result a better energy resolution. Reflections from the sides of the crystal, scattering inside the crystal and statistics of scintillation light all distort the LRF, which results in spatial loss due to harder position estimation (Figure 23. Limitation factors in crystal slabs).

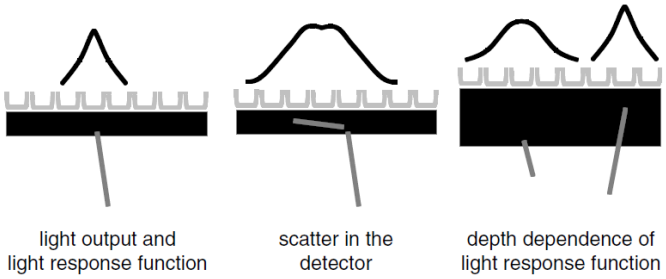

Figure 23. Limitation factors in crystal slabs (Lewellen, 2008)

3 SPADNET

The SPADnet project started in 2010, with the involvement of European universities and research centers. It takes aim at the development of a scalable network of imaging sensors for biomedical applications. The sensors are sensitive light detectors built up from SPADs, fabricated using conventional CMOS technology (SPADnet project, 2010).

3.1 SPADNET SENSOR

SPADnet sensors are digital SiPMs, based on so called Mini-SiPMs. Mini-SiPMs are the smallest elements handled individually in the device, containing a number of SPADs. Applying certain technological methods, mini-SiPMs are favourable from both the aspects of increased fill factor, and the desired low DCR which would increase with larger SPADs. There is a special spatial and timing compression utilized on signals of the SPADs in the device, thus SPADs of a certain mini-SiPM could be accounted with the same resources of the mini-SIPM (e.g. digital counter), even during the dead time of another SPAD. Hence, the connected SPADs act like a bigger SPAD regarding the size of the sensitive area, while having a DCR low as for one single SPAD (H. C. Braga, et al., 2011).

The first generation of sensor carried out in the project (SPADnet1) is built up using 16x8 pixels, each pixel containing 4 mini-SiPMs. A single mini-SiPM contains 180 SPADs, which results in 720 SPADs per pixel, and 92160 SPADs on the whole sensor (Figure 24. SPADnet1 sensor. Sensors can be built up to a tile of 5x5 sensors. These tiles form the detectors of the detector ring.

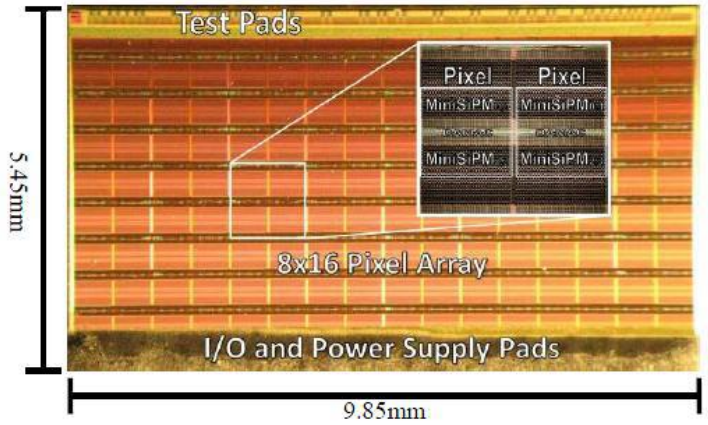

Figure 24. SPADnet1 sensor (Walker, et al., 2013)

The sensor works as follows. During operation, photon counts on the whole surface are integrated for 10 ns intervals. This sum (noted as energy, since it is proportional to the energy absorbed in the crystals) is available at the end of each interval on a 16 bit bus. The energy is continuously compared to a predefined threshold value (which can be adjusted from outside of the chip). If energy crosses the threshold, integration is continued to a longer (adjustable) time. After integration the spatial distribution (number of impinged photons on each pixel), the energy, and the TDC values are available on the dedicated output of the chip.

This sensor has other significant features, like filtering of pile-up events (events, when more than one gamma photon is absorbed in the crystal, preventing positioning possibilities), filtering of scattered events, per SPAD disallowance to reduce noise, etc…). The chip is available with test pads for easy characterization, while it is also available using through-hole-via design, which enables a high fill factor when sensors are assembled to a tile. Further processing is carried out on an FPGA connecting to the sensor, implementing the firmware for the device.

By the time of this writing, characterization of the second generation SPADnet sensor (SPADnet2) is being carried out. The second generation sensor has 16x16 pixels, further built-in processing, and other improvements.

3.2 SIMULATIONS

Positioning investigations were carried out on simulated data. The simulations were performed using the Zemax and Matlab software in two steps. In the first step the scintillator crystal configuration has been simulated using Zemax. The simulated behavior takes account of several properties of the construction, the geometrical configuration of the crystal, the material of the scintillator, the structure on the sides of the crystal, etc. The output of simulations consists of a dataset with the information of light photons that are generated for different positions of gamma photon interactions. This data is then processed by Matlab scripts in the second step, where the behaviour of the light detector device (the SPADnet light sensor) is built into the data set. This is based on the SPADnet sensor taking into consideration detailed parameters including circumstances of real operation. The final output for the simulations consists of photon counts on each pixel of the SiPM for given gamma photon interactions (in data files), but without any timing information, and certain information on geometric configuration of the sensor (coordinates and size of pixels and sensors of the tile in a text file).

The simulated crystal is a crystal slab with polished side optically coupled to a light guide on the side of the sensor, retroreflector on the back side, and reflective surfaces on the sides. The simulation of light sensor incorporated the features of the first generation SPADnet chip according to its specification and behavior but with simulating 16x16 pixels (the size of the second generation chip). There were 5x5 planar positions and 3 depth levels of gamma photon interaction simulated on a sensor tile of 5x5 sensors. In each of the resulting 75 POIs 100 interactions are simulated (Figure 25). Three representative planar positions out of the twenty-five planar test points are marked with red colour. These are the 3x3 test points (three planar positions in each of the three simulated depth level) in which I evaluated the certain algorithms.

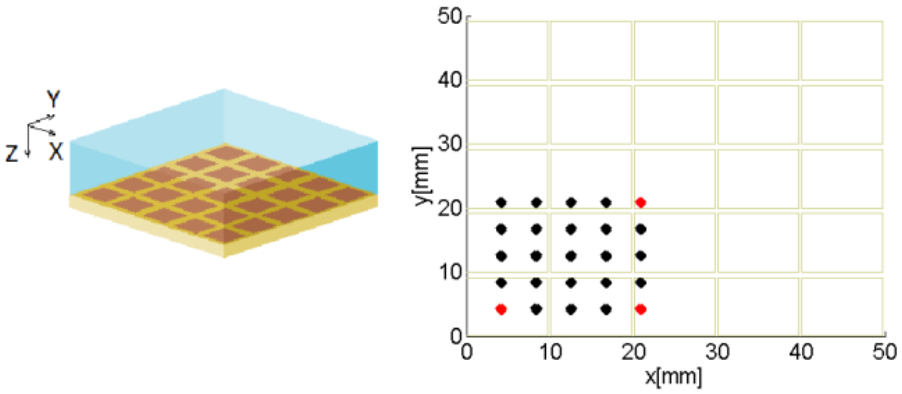

Figure 25. Simulated configuration, and simulated POIs

3.3 COG ALGORITHM

In a previous work I investigated possible algorithms to utilize with SPADnet sensors. Although more complex algorithms were taken into consideration as well (Ling, Lewellen, & Miyaoka, 2007; van Dam, et al., 2011; Joung, Miyaoka, & Lewellen, 2002), I mainly focused on simple and fast solutions in order to be able to implement the algorithm on an FPGA connected to the sensor. Another viewpoint was to provide real time positioning, even for frequent gamma photon interactions. As a result I chose a COG based method. The COG method with data of a digital SiPM looks like the following:

$$x_{COG} = \frac{\sum_{i=1}^{N} p_i x_i}{\sum_{i=1}^{N} p_i}, y_{COG} = \frac{\sum_{i=1}^{N} p_i y_i}{\sum_{i=1}^{N} p_i} \quad (4)$$

N denotes here the number of pixels, x_i, y_i and p_i are the x and y coordinates, and the photon counts of the *i*-th pixel. This is a weighted average of the pixel coordinates, where the weighting coefficients are the detected photon counts on the pixels.

However, because of the distorting effect on the sides, the detector noise and other uncertainties, the COG estimation gets unacceptably imprecise close to the detector edges and corners. This can be seen in the three representative points mentioned earlier, in the three depth levels, where COG was calculated for twenty simulations in each test points (Figure 26). This is understandable, since noisy

pixels which only have a few counts (dark counts) could strongly modify the weighted sum, if the pixel is far away from the POI. When the POI is in the middle of the detector, this is not a problem since these noisy pixels surround the POI from all directions. In the case when the POI is closer to the edge or the corner of the detector surface, noisy pixels affect the weighted coordinate only towards a certain direction (the middle of the sensor). Thus, some kind of noise reduction is expected to overcome this issue.

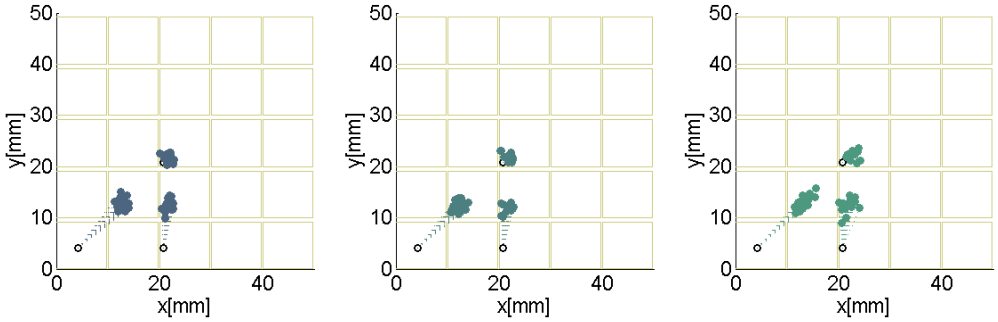

Figure 26. COG (z = 0.500 mm, z = 5.000 mm, z = 9.500 mm)

Normally, this would be done by expecting the photon counts on the pixels as observations of light photons (with respect to a certain light response function of the scintillator crystal) and an additional noise (dark counts). In this model, the necessary step is to subtract the expected value of noise (transformation of the random variables so the expected value of noise becomes zero). The expected value could be approached by determining the pixels, which would not detect scintillation light photons (since the light photons generated in a gamma interaction does not spread over the whole surface) and then calculate a mean of photon counts of these pixels. In case of the SPADnet sensors this is problematic, since (as described earlier) output is only generated if the detected energy crosses a certain threshold. If the number of detected counts (including dark counts) is under this threshold, there will be no output generated (namely say, the sensor acts as if it was blind). Statistical fluctuations in the number of dark counts (and the number of incident scintillation photons if there are any) causes a few sensors of a tile to have zero as detected photon count for each pixel because of not crossing the threshold, even if neighbouring sensors do have a noisy output. This is even visible on simulations (marked with red rectangular on Figure 27)

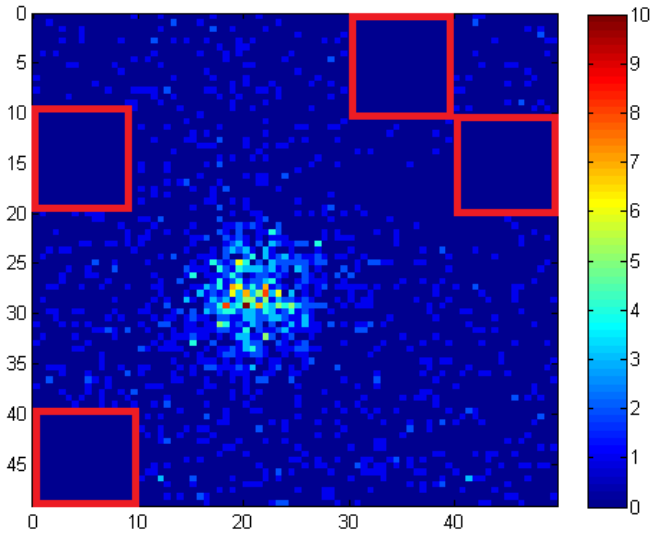

Figure 27. "Blind" sensors of a tile

Because of this, only pixels of sensors which are not completely blind, but still (probably) not hit by scintillation light photons has to be taken into consideration when calculating a mean. This could be simply done by only accounting sensors which have at least one positive photon count, while all the photon counts are under a certain (empirical) threshold. Unfortunately, this method cannot explore noisy pixels only, since when a “tail” of the light response function is above a different sensor than the POI, low number of scintillation photons of the tail could be considered as noise. Because there is a small dead area between the neighbouring sensors, and this phenomenon concerns only a limited number of pixels, it is expected that it has a negligible impact on the mean. Nevertheless, because of statistical fluctuation of the light response function there is a small chance, that a photon count on a sensor is caused by a real scintillation photon, and not by dark current, which sensor is otherwise only affected by noise (the same effect as the one above, but further away from the POI). Because of the low probability of this to happen this has no significant effect on the mean either. Applying this noise reduction method resulted in a much better estimation (Figure 28).

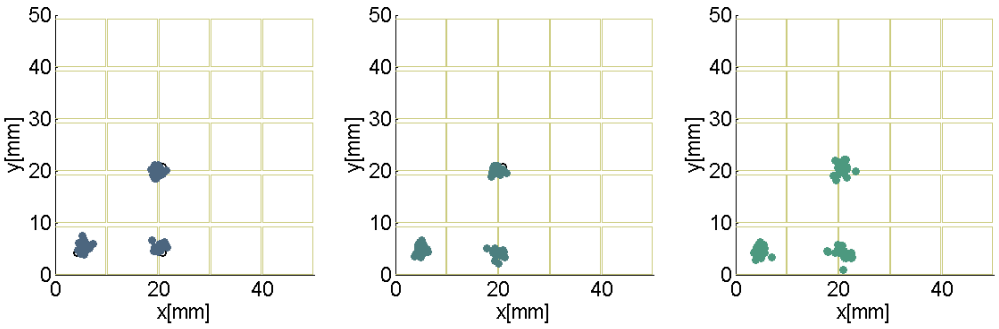

Figure 28. COG with noise reduction (z = 0.500 mm, z = 5.000 mm, z = 9.500 mm)

The improvement is clearly visible on the figures, without any numerical analysis. However the achieved accuracy could slightly be increased. For this I applied a certain threshold over the whole surface of the sensor. Values that are under this threshold were considered as zero (marked with blue on Figure 29).

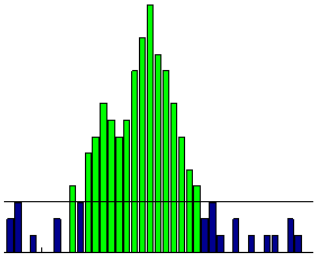

Figure 29. Applying a threshold

Normally this technique should be avoided, since its causes a non-linear transformation on the random variables of photon count observations, as the noise of sensor is still present on pixels which are affected by enough scintillation light to cross the applied threshold, depending on the POI. From this point identical distribution of the random variables won't be true, which would hinder the efficiency of any further processing. However, it is still considerable if no further processing is planned, as it achieves a slightly better accuracy regarding these exact simulations. On the other side, in a case of a scintillator array, this sort of positioning technique might not be the best, but it is good enough if it results in a simple segmentation demand. Current measurements have shown that by choosing a good threshold value, the estimated positions had an offset from the center of the crystal

surface in the order of a tenth millimeter with very low variance (Játékos, Lőrincz, Ujhelyi, & Erdei, 2013). Another benefit is that it is easier to be implemented on an FPGA and have a shorter computational time (lacking the mean calculation). A drawback is the need for calibration before real measurements to set a good threshold. Figure 30 was carried out with a threshold of 2 photon counts based on an experimental comparison of different values.

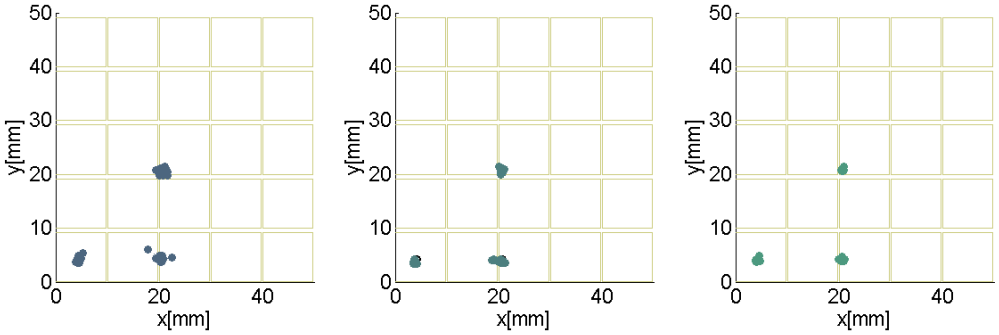

Figure 30. COG with threshold (z = 0.500 mm, z = 5.000 mm, z = 9.500 mm)

4 MLE METHOD

The COG algorithm was chosen to be utilized because its simplicity. Considering the aim of PET systems, at the end of the day we would like to reach a better and more accurate diagnostic image. Since the method has the drawback of putting a patient through to radioactive irradiation, a better image is needed with restrictions of a safe and harmless operation. This limits the amount of the applied radiotracer, although a higher number of annihilations would infer a more accurate image. As a consequence, any solution which achieves a more accurate image reconstruction is reconsiderable. With respect to positioning, a better positioning ends up in better designation of LORs. This way more precise LOR designation could redeem the benefits of having a higher number of LORs.

Certain properties of the maximum likelihood estimation provide that it is the theoretically best estimation method, which means that it could extract the most information from a dataset compared to other methods. This way it can be thought as a benchmark to compare against. My intention with the implementation of the ML method for positioning is to decide, whether the described COG needs further improvement, or if it is worth to seek for even better solutions.

4.1 BASICS OF MLE

The key of MLE is to estimate the most probable parameters of a statistical model, which could result in a certain dataset of observations. In other words, the task is to identify a certain population which is most likely to have generated a given observation. Mathematically expressing, let's consider a random vector of observations $X_1,...,X_i,...,X_n$, with each having a parameter ($\overline{\vartheta} \in \Theta, \Theta \subset R^m$) dependent probability density function $f_i(x \mid \overline{\vartheta})$. This is also called the parametric model. In case when the samples are independent, and identically distributed, their joint density function over the n-dimensional space could be expressed as:

$$\prod_{i=1}^{n} f_i(x \mid \overline{\vartheta}) = f(\overline{x} \mid \overline{\vartheta}) \qquad (5)$$

For fix observations ($x_1,...,x_i,...,x_n$) we define the likelihood function as a function of $\overline{\vartheta}$, depending on the parameter $\overline{x}$:

$$L(\overline{\vartheta} \mid \overline{x}) = f(\overline{x} \mid \overline{\vartheta}) . \tag{6}$$

A $\hat{\overline{\vartheta}}$ that maximizes the likelihood function over Θ is called a maximum likelihood estimate of the unknown, true parameter: $\overline{\vartheta}$.

ML estimators have several desirable properties:

- asymptotically unbiased, this means, that the ML estimators converges to the real parameter value in probability, when sample sizes are increasing towards infinity,
$$P(\overline{\vartheta}_{MLE} = \overline{\vartheta}) = 1, \tag{7}$$
- asymptotically normal, this means, that the distribution of ML estimators tends to normal distribution, when sample sizes are increasing towards infinity
- efficiency, this means that it reaches the Cramér-Rao lower bound, when sample sizes are increasing towards infinity. This basically means, that no other estimator achieves a lower mean squared error
- invariance to transformations, this means, that ML estimator of a function on random samples will be the function value at the ML estimator of the random samples.

It is worth to mention that the ML estimator does not necessarily exist. Sometimes from a computational point of view it is easier to calculate the log-likelihood function:

$$l(\overline{\vartheta} \mid \overline{x}) = \log L(\overline{\vartheta} \mid \overline{x}) \tag{8}$$

This could be done, since the logarithm is a strictly monotonic function and thus has its extrema at the same point as the argument (the nested likelihood function in this case).

4.2 THE APPLIED MODEL

In the case of the SPADnet sensor for a proper model to apply let's consider a gamma interaction with total absorption in a crystal of unlimited sizes. As the crystal is isotropic, and assuming no defect or irregularity of the crystal, the medium in which scintillation photons spread could be considered completely homogenous. This means that the probability for a photon to spread towards a certain

direction has rotational symmetry. Taking into consideration the above stated premises, the probability density of gamma photons hitting the surface is a two dimensional curve with rotational symmetry. If we look at simulated gamma interactions in the middle of the crystal in different depth levels, this seems to be a good starting point (ignoring noise in the first step, Figure 31). Note, that dead areas are not shown on the figures (more specifically the center of pixels on the figures are matching their real geometrical position on the real device, but photon counts are depicted as if pixels were connecting directly without dead space between).

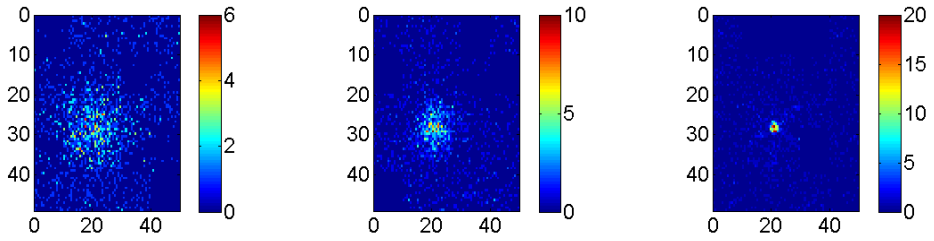

Figure 31. Typical light distributions for gamma interaction at different depth levels (z = 0.500 mm, z = 5.000 mm, z = 9.500 mm)

It is seen on the figures, that for an interaction further away from the detector surface (z=0.5 mm) light photons have a higher spread reaching the detector. This results in a higher number of firing pixels with a lower photon count compared to scintillations close to the sensor (z=9.5 mm) where there is a fewer number of firing pixels with a higher photon count.

For an initial step, I assume this two dimensional curve to be a 2D Gaussian curve. The reason for this is that it is easy to manage and calculate with, and on the other hand, I am firstly interested in the position of the gamma interaction, which is the center of this curve (the peak), just as for any other two dimensional curve with rotational symmetry, that could be assumed instead (namely, for a given interaction, the resulted light distribution with rotational symmetry could be more probably described with a different rotationally symmetric probability density function with the same center position compared to its real density but with wrong center position). From this point I build in more and more known details of the detection process into the model. Most of the time, these are approximations of the real process with a manageable mathematical apparatus.

4.2.1 PHOTON NOISE

The first thing that should be clearly presented in the model is noise. We might think of the photon count at a certain pixel, as a number of photons from all generated photons. This photon count is reached according to a parameter describing the expected value of the number of photons from all generated photons that are chosen for this specific pixel. This expected value is depending on the POI. The number of all generated photons changes for each interaction, thus a binomial distribution (of the number of detected photons over a pixel) would be different for each gamma interaction, even if it had the same POI. Nevertheless, the probability of a specific light photon from all photons to impinge on a certain pixel is relatively low. Because of these, I assume that photon counts have a Poisson distribution over each pixel, with different and POI dependent expected value. This expected value is exactly the integral of the 2D Gaussian density function over the certain pixel. This is depicted on Figure 32 in one dimension.

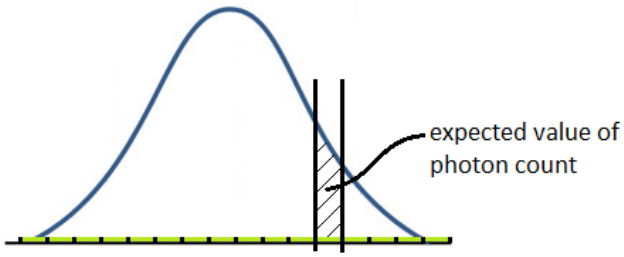

Figure 32. The calculation of the expected photon count

So far our model is that photon count observations at pixels have a Poisson distribution, which distributions are dependent on the density function of the light distribution. The 2D Gaussian curve can be generally written as:

$$f(x,y) = A \cdot e^{-(a(x-x_0)^2+2b(x-x_0)(y-y_0)+c(y-y_0)^2)} \tag{9}$$

where $\begin{bmatrix} a & b \\ c & d \end{bmatrix}$ is positive-definite. In a particular case when the curve is rotationally symmetrical, this could be written as:

$$f(x,y,) = A \cdot e^{-\left(\frac{(x-x_0)^2}{2\sigma^2}+\frac{(y-y_0)^2}{2\sigma^2}\right)} \quad (10)$$

where A is the amplitude, x_0, y_0 is the center position, σ is the spread of the blob.

With this, our random sample consist of the photon counts with Poisson distributions depending on the parameter vector A, x_0, y_0, σ. This way the channel characteristics of the detection process could be considered as a transformation from the four dimensional parameter space to the 6400 dimensional (80x80 pixel of the tile) observations.

The MLE method is based on the determination of the likelihood function using our model. It is seen that the likelihood function is formally the same as the joint probability density function of the random samples but over the parameters of the density functions having the observations as parameters. Thus it is needed to determine the joint probability density function. Unfortunately, the distributions of the photon counts are not independent from each other, since they are connected through the light distribution probability density function. Talking about the identity, they have the same family of distribution (the Poisson distribution), but with different expected values. As a result, with an approximation they could be considered as their observed values moves around their expected values almost the same way, but independently from each other. This way, the joint probability function is calculated as a product of the Poisson distributions. This means, that the value of the likelihood function for a given parameter is the product of probabilities of observing certain photon counts over the pixels. These probabilities are calculated with respect to the distribution of the photon counts.

4.2.2 LIGHT SENSOR NOISE

This model apparently is not complete. Considering pixels far from the POI, the integration of the probability density function (PDF) of the light distribution results in an expected value that is almost zero, let's consider it zero. Poisson distribution with zero expected value (and thus zero variation)

assumes a random variable with a value of zero, with one probability. Still we see pixels with photon counts other than zero (dead count).

Assuming a Poisson distribution for dead counts as well, the observed photon counts have a distribution that is the sum of two Poisson distributions. The expected value of the sum of Poisson distributions is the sum of the expected values of each Poisson distribution. Assuming that the distribution of dead counts is the same for all pixels on the sensor surface with the same expected value, this can be built in our model, by adding a constant offset to the light distribution PDF (from now on this will be denoted as photon count probability density function).

$$f(x,y,) = A \cdot e^{-\left(\frac{(x-x_0)^2}{2\sigma^2}+\frac{(y-y_0)^2}{2\sigma^2}\right)} + C \qquad (11)$$

where the integral of C over the pixels will give the expected value of sensor noise. It is worth to mention, that if we are able to estimate our parameter vector, it is possible to estimate not only the POI, but the sensor noise and the DOI as well (which could be calculated from the amplitude and the spread parameters).

4.2.3 CRYSTAL EDGES

If we calculate the ML estimates of the parameters (the technique for that is described later) we could see, that the estimated position is incorrect when the POI is close to the sensor corner or the sensor edge, especially when the depth of interaction is further away from the crystal (in these cases the light photons create a wider “spot” on the sensor surface, as mentioned before) Figure 33 depicts ML estimates of the POI coordinates for twenty simulations, at the three representative points et three depth levels.

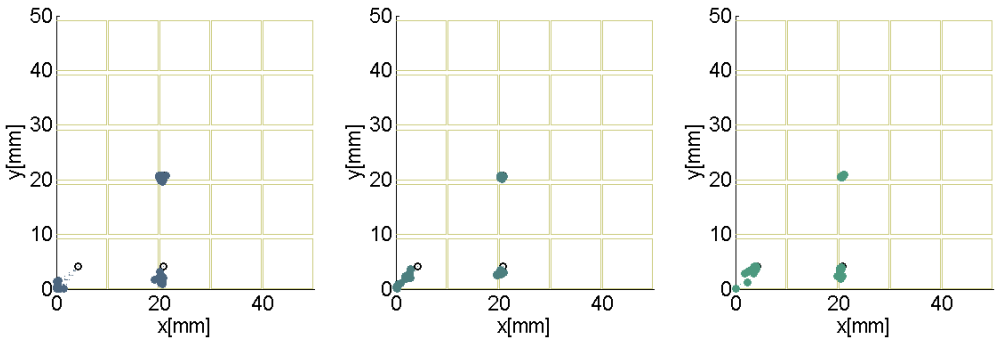

Figure 33. ML estimates of POI (z = 0.500 mm, z = 5.000 mm, z = 9.500 mm)

The reason of this either could be an incorrect applicatiom of MLE (incorrect calculation), or an error in the model. It seems that the estimation is deteriorated especially when the relevant part of the light distribution PDF reaches the detector edge. For this, I tried to build the effect of the reflective edges of the crystal into the model.

For this, I concerned with the PDF of the photon count distribution not only above the detector, but on a bigger surface. The size of this bigger surface was chosen with considerations on the spread of the light distribution PDF. Namely, according to the simulations, it can be seen, that the light spot typically has a limited spread (Figure 31). The extra size beyond the detector surface I dealt with was chosen to include the relevant part of the PDF even for POIs close to the detector edge. (The expression “relevant part” is used since in case of a Gaussian curve the probability of photons hitting the surface won’t be exactly zero, even far away from the POI. However, after a certain distance from the POI it is negligible). Having the PDF over the bigger surface, I reflected the photon count distribution PDF at the edges, and summed it up over the sensor (this could be imagined as folding back the PDF on the detector edges) (Figure 34).

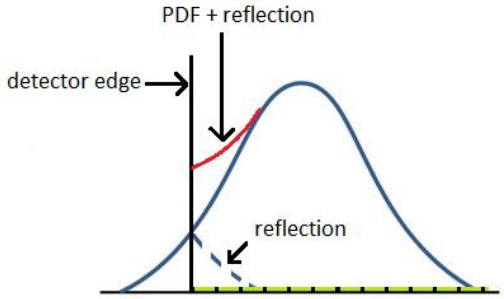

Figure 34. PDF reflection on the detector edge

I only implemented this solution on the sides of the detector and not in the corners (for computational reasons) (Figure 35). This means that photons, which would reflected twice in the corners are not accounted (Figure 36). On the other hand, I reflect the PDF of the photon count distribution, not the light distribution PDF (for an easy and quick calculation, since these values are already calculated), however this way a higher number of dark count is expected on the edges. Hence, this is not a completely correct solution of accounting the reflective crystal edges, still it might supposed to have an improvement on the estimation.

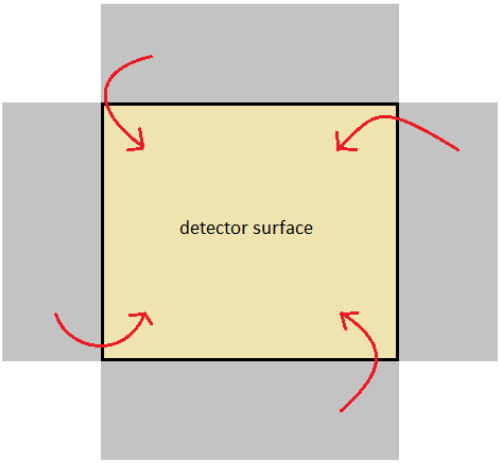

Figure 35. Reflected areas

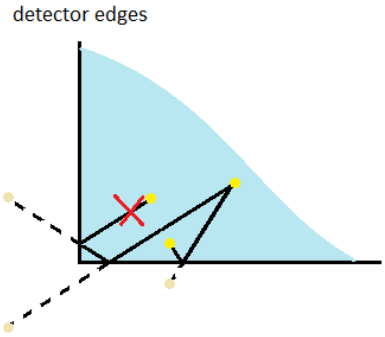

Figure 36. Light photon reflection in the corner

The calculated ML estimates show that we indeed have better estimations.

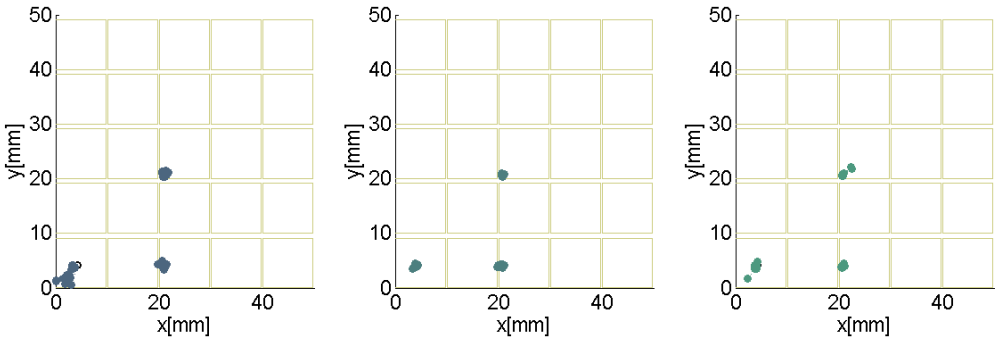

Figure 37. ML estimates of POI when reflections are accounted (z = 0.500 mm, z = 5.000 mm, z = 9.500 mm)

4.2.4 BLIND SENSORS

We considered the effect of noise, but the model does not describe the simulations correctly. It is already mentioned, that because of the working principles of the SPADnet sensors, certain sensors will be “blind” in gamma interactions. If this is not accounted, than the estimated expected value of dead counts (previously noted as C parameter in (11)) will be incorrect, since it is assumed, that the observed values of dead count were zero on several pixels (corresponding to “blind” sensors). This way, if we would like to include this phenomenon into the model, sensors with no output has to be

found, and the probability of observing zero over their pixels has to be set to one. Indeed, In this case, the expected value of dead counts is not uniform on the whole surface, on blind sensors it is zero. By observing zero photon counts on these pixels means that the probabilities of the observations are one.

Setting the observation probabilities to one on pixels of the blind sensors, we achieve an even more accurate estimation (Figure 38).

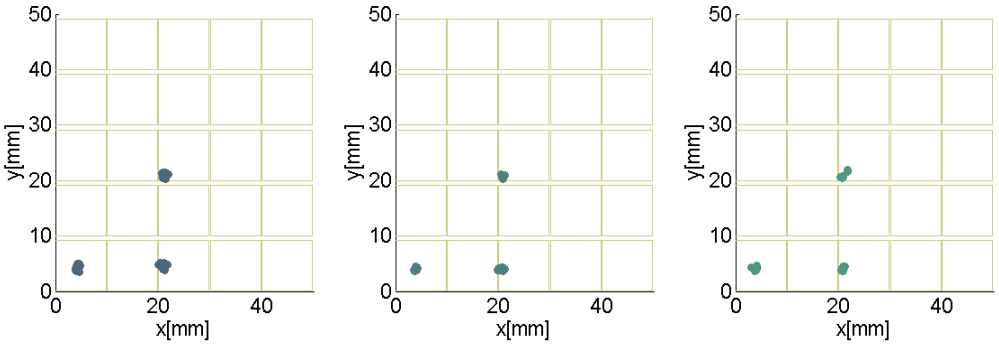

Figure 38. ML estimates when blind sensors are accounted (z = 0.500 mm, z = 5.000 mm, z = 9.500 mm)

4.3 DE OPTIMIZATION

In MLE the first step after specifying the applied model is to determine the likelihood function. The next step is to find the maximum of this function, which means, finding the most probable parameter that have generated the observations.

In the previous subsection I introduced the model of which the likelihood function can be determined with. As it has been mentioned, the model consisted of Poisson distribution of the photon counts over the pixels. It has been stated as well, that we approximate the likelihood function with the product of the Poisson distribution, and hence the likelihood function value is the product of the photon count observation probabilities.

A key step in the likelihood function was the two dimensional integration of the photon count PDF. For simple calculations and a reasonably fast algorithm I approximated these integrals with a value, which is proportional to the PDF value at the center of the pixel.

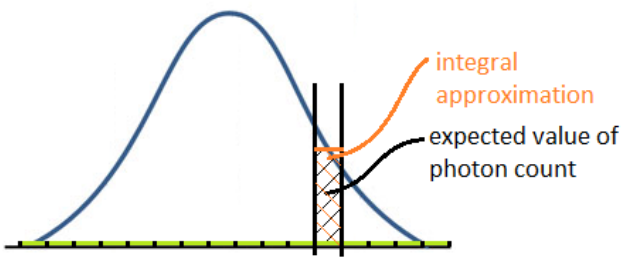

Figure 39. Approximation of the integral

For this I deal with a 2D Gaussian curve proportional to the photon count distribution PDF as if it was multiplied at each argument with the size of a pixel. Thus, the value of this Gaussian curve at the center of a pixel gives the approximation of the integral of the PDF over the pixel. When working on the estimated parameters, one should keep in mind to transform them back to the original PDF, if the original parameters of the PDF are desired. In my case, I am only interested in the center of the curve, which is the same for the original PDF and to its proportional Gaussian curve, and so I don't deal with the PDF, only with its proportional Gaussian curve. (Note that if for example the expected value of the dead count (C parameter) was needed, it is exactly the C parameter of this proportional curve, as it is the integral of the C parameter of the original PDF (11) over the pixels).

Performing the "integration" we get the expected values of photon counts. The probabilities of the observations can be then calculated, knowing that the counts follow Poisson distributions:

$$P(X = k) = \frac{\lambda^k}{k!} e^{-\lambda} \tag{12}$$

where X is the photon count variable, k is the observed photon count and λ is the expected value calculated from the photon count distribution PDF.

The probabilities have their values between zero and one. There is 80x80 pixels on the sensor surface, thus the product of probabilities will be a very low number. In order to be able to carry out numerical calculations using double precision numbers, some kind of transformation is needed on the probabilities. This is exactly something what the log-likelihood can overcome. Calculating the (natural) logarithm of the probabilities, a probability of one will be zero and lower probabilities will

be negative numbers accordingly until the probability of zero, which logarithm is negative infinity. The product of these will be negative, and because of this the log-likelihood function is often multiplied with minus one, and accordingly the most probable variables (parameters of the model) could be found as minimum values of this function.

For finding the extrema, usually a gradient method is applied. Because of the complexity of my likelihood function I chose another way instead, which was the utilization of the Differential Evolution (DE) algorithm (Storn).

This is an algorithm for optimization, which does not require the gradient of the objective function. It works by maintaining a population of possible argument variables (candidates) and iteratively creating new candidates by combining existing ones (adding weighted difference of two population members to a third). The algorithm has proved to be useful and effective for different optimization problems. The drawback of the method is that it is not guaranteed that an optimal solution (a best candidate) is ever found (Storn).

The source code of the DE algorithm can be freely downloaded for several programming languages. The downloaded code than could be modified to fit ones certain problem. It has several properties that could be set for a better performance (number of population members, number of iterations, the weight to use when generating the mutant population, etc…). I set these properties based on experiments using the algorithm to have an optimization which avoid sticking in local extrema of the likelihood function and has a reasonable long time to surely find the extrema. This also required to set up certain constraints on the possible values of the parameters. I set up these constraints according to the detector configuration (e.g. the POI cannot be a position outside of the detector surface), and empirical findings (e.g. the σ parameter cannot be higher than a certain number according to simulations). Starting the algorithm with an initial population which consisted of candidates close to the true parameters the algorithm proved to have a relatively quick procession (in the order of a second). This was done by applying a simple previous estimation and setting limits for the initial population, e.g. in case of the POI I set these limits around the maximum photon count.

4.4 EVALUATION

With including all the previously described effect into the model, and searching the most probable parameter using the DE method, I could calculate the maximum likelihood estimates of the POI. For a comparison of the COG based method with the MLE method I calculated the average (13) and the corrected sample standard deviation (14) of the distance between the estimated position and the real POI for 20 simulations at each of the three representative planar points (middle, edge, corner), at each of the three depth levels (z = 0.500 mm, z = 5.000 mm, z = 9.500 mm). These values express the bias and the square root of corrected sample variance of the position estimator.

$$\bar{d} = \frac{1}{N}\sum_{j=1}^{N} d_i \tag{13}$$

$$\sigma_d = \sqrt{\frac{1}{N-1}\sum_{i=1}^{N}(d_i - \bar{d})^2} \tag{14}$$

For the COG based method these are the following:

Bias of estimation (mm)

corner			***edge***			***middle***		
z = 0.5	***z = 5.0***	***z = 9.5***	***z = 0.5***	***z = 5.0***	***z = 9.5***	***z = 0.5***	***z = 5.0***	***z = 9.5***
0.51	0.57	0.32	0.75	0.73	0.33	0.73	0.47	0.25

Unbiased standard deviation of estimation (mm)

corner			***edge***			***middle***		
z = 0.5	***z = 5.0***	***z = 9.5***	***z = 0.5***	***z = 5.0***	***z = 9.5***	***z = 0.5***	***z = 5.0***	***z = 9.5***
0.33	0.15	0.20	0.78	0.53	0.23	0.37	0.23	0.13

For the MLE method, these are:

Bias of estimation (mm)

corner			***edge***			***middle***		
z = 0.5	***z = 5.0***	***z = 9.5***	***z = 0.5***	***z = 5.0***	***z = 9.5***	***z = 0.5***	***z = 5.0***	***z = 9.5***
0.41	0.30	0.48	0.50	0.38	0.41	0.54	0.23	0.41

Unbiased standard deviation of estimation (mm)

corner			***edge***			***middle***		
z = 0.5	***z = 5.0***	***z = 9.5***	***z = 0.5***	***z = 5.0***	***z = 9.5***	***z = 0.5***	***z = 5.0***	***z = 9.5***
0.25	0.18	0.18	0.34	0.29	0.07	0.19	0.14	0.32

We can see that the ML estimates generally prove to be more accurate with respect of bias and unbiased standard deviation. In fact, in certain points it seems less accurate than the COG based

method. This could be because of statistical uncertainties of the low number of simulations we investigated, but shows that the two methods have results close to each other. The task is now to decide, whether this improvement is worth using a much more complex estimation solution. It has been indicated that a better estimation of the POI results in a better resolution on the FOV. However, we have to keep in mind all other uncertainties which are limiting the overall performance. Looking at the results, the MLE outperforms the COG based method with a few tenths of millimeters. Even if we chose a more accurate model and try to apply better approximations, this is not supposed to be much better (the difference of the two methods will still be in this magnitude). Being aware of the limiting factors in image reconstruction, we can say, that having a more precise positioning with a few tenths of millimeters this won't infer measurable reduction in the amount of needed radiotracer.

The fact, that the COG based method has its benefits in low computational complexity and short time of processing, it could be considered as a rather acceptable solution for positioning.

4.5 FPGA IMPLEMENTATION

In order to have a feeling on FPGA implementation possibilities, we have to review the requirements that MLE stands. Floating point calculations do not mean heavy restrictions, however there are several crucial points of the ML method, that hinders an efficient FPGA implementation. First of all, calculations with the exponential function. Since our model includes a 2D Gaussian curve, it is inevitable to carry out calculations with the exponential function. There are several studies investigating better and better solution for exponential calculations on FPGAs, since this function plays a key role in many scientific problems (Sudhaa , Hanumantharajub, & Venkateswarulua, 2012; Yuan & Xu, 2013). Without depicting a certain solution it could be said, that based on the implementation method, a complex module requires a few thousand number of slices, including several DSP slices as well. The time of the operation is dependent on this accordingly, it is usually a few hundred cycles, but not less than a few tens. Taking into consideration a clock sign in the order of 100 Mhz, this means a few microseconds of calculation. Another question is the accuracy of the output of exponential calculation, since many of these methods use approximations.

Another critical point is the integration, but using the same technique as described in this report, it could be avoided by approximations.

Unfortunately, the Poisson distributions require exponential calculations again. For all the pixels, this would be in the order of a few milliseconds. This might be avoidable, by changing the applied model. In an approximation we could use least square estimation, but in that case the approximation might not result a more accurate solution compared to the COG method. Weighted least squares might result better then least squares, but it means no (or not relevant) computational benefit if the weight is calculated as standard deviation of the distribution, since it can be calculated by determining the mean value of the Poisson distribution.

Then next problem is we either have to have huge precision for the product of probabilities or we have to calculate logarithm. With certain solutions the logarithm calculation needs lower amount of resource than for the exponential calculation (Alachiotis & Stamatakis, 2010; Tropea, 2007).

The most critical part is the extrema finding of the cost function. Considering iterative solutions, this means that the estimated computational time is multiplied by the number of iterations. Otherwise, we could set up a number of points in the parameter space where we would like to calculate the cost function, and then simply choose the one with highest probability (lowest cost). This way, a tradeoff can be made between computational complexity and achievable resolution with adjusting the number of points in the parameter space to use. Let's consider that the real POI is pre-estimated by a simple solution (this could either be the modified COG). After that, we can set up the parameters points around this pre-estimated position with the desired resolution. Considering a five dimensional parameter space, only a few predefined points for each parameter results in a huge number of points in the parameter space.

Either use iterations or a predefined number of points in parameter space, calculating the cost function for let's say a hundred times is in the order of a few tenths of a second. If we have incident gamma photons in a number of 10^6 per second on the whole detector ring (which is a typical value), there is no chance for live processing of the data with this implementation..

Only if these are just initial thoughts without real investigations about feasibility, these clearly indicate, that there is no point in FPGA implementation of such a comlex and resource oriented method as the MLE, especially, if a much simpler (COG) method provides almost the same results.

5 SUMMARY

In this report I investigated a maximum likelihood based estimation technique for gamma photon position estimation in PET detectors. Using approximations in the modeling process the results have showed, that the implemented ML method only outperforms a simple COG based method with a few tenths of millimeter. Taking into considerations other factors which are limiting the efficiency of the image reconstruction, and keep in mind the differences of computational efforts of the methods it can be said, that there is no point in applying MLE method instead of the described COG based method.

FPGA implementation considerations also confirm this statement.

With different hardware setups (e.g. using DSPs instead of FPGA) it could be a future study to investigate possible MLE implementations. This not only requires an effective implementation of the MLE method, but to be able to reach an even more accurate MLE, which is worth implementing instead of the COG. For this, a better understanding of the detector setup is needed, in order to be able to build up a more accurate model. This includes better modeling the effects of the reflective edges, the effect of the retroreflector on the back side of the crystal, and investigations, whether a different curve with rotational symmetry better describes the light distribution than a 2D Gaussian curve.

ACKNOWLEDGEMENT

I would like to thank Dr. István Kollár for constructive conversations, help and ceaseless guidance. I also would like to thank Dr. Emőke Lőrincz and Balázs Játékos for their assistance and guidance, as well as for submitting materials and simulation data for the investigations. This report connects to the EU FP7 project SPADnet. I would like to thank the help of all partners and colleagues of the project for their help.

LIST OF FIGURES

REFERENCES

A 2D Positioning Application in PET Using ANNs (Artificial Intelligence). (n.d.). Retrieved 10 10, 2014, from what-when-how: http://what-when-how.com/artificial-intelligence/a-2d-positioning-application-in-pet-using-anns-artificial-intelligence/

Alachiotis, N., & Stamatakis, A. (2010). Efficient floating-point logarithm unit for FPGAs. *IEEE International Symposium onParallel & Distributed Processing, Workshops and Phd Forum*, (pp. 1-8).

Bassignanaa, D., Fernandez, M., Jaramillo, R., Lozano, M., Munoz, F. J., Pellegrini, G., et al. (2012, February). First investigation of a novel 2D position-sensitive semiconductor detector concept. *Journal of Instrumentation*.

Bird, A., Ramsden, D., & He, Z. (1994). Multi-channel readout of crossed-wire anode photomultipliers. *Nuclear Instruments and Methods in Physics Research A*, 668-672.

Casey, M. E., & Nutt, R. (1986, február). A Multicrystal Two Dimensional BGO Detector System for Positron Emission Tomography. *IEEE Transactions on Nuclear Science, 33.*(1.), 460-463.

Fontbonne, J.-M. (2013, April 3). Time of flight and position measurement using a MCP with resistive position readout. Caen, France.

Frederic H. Fahey, D. (1. June 2002). Data Acquisition in PET. *Journal of Nuclear Medicine Technology*, 39-49.

H. C. Braga, L., Pancheri, L., Gasparini, L., Perenzoni, M., Walker, R., Henderson, R. K., et al. (2011). A CMOS mini-SiPM detector with in-pixel data compression for PET applications. *IEEE Nuclear Science Symposium Conference Record* (pp. 548-552). IEEE.

Hamatsu. (2006). *Photomultiplier Tubes - Basics and Applications.* Hamatsu Photonics K. K.

Ishii, K., Kikuchi, Y., Takahashi, K., Nakamura, K., Matsuyama, S., Terakawa, A., et al. (2011). *Nuclear Instruments and Methods in Physics Research A*, 138-143.

Játékos, B., Lőrincz, E., Ujhelyi, F., & Erdei, G. (2013). High probability cristal pin identification in scintillator matrix-based PET detector with a prototype digital SiPM. *(due)*.

Joung, J., Miyaoka, R., & Lewellen, T. (2002, August 21). cMiCE: a high resolution animal PET using continuous LSO with a statistics based positioning scheme. *Nuclear Instruments and Methods in Physics Research Section A: Accelerators, Spectrometers, Detectors and Associated Equipment*, 584–598.

Kroeger, R., Grove, J., Inderhees, S., Johnson, W., Kinzer, R., Kurfess, J., et al. (1997). Thin Scintillators and Position Sensitive Photomultiplier Tubes for Hard X-ray Imaging in Space. *IEEE Transaction On Nuclear Science*.

Lewellen, T. K. (2008). Recent developments in PET detector technology. *Physics in Medicine and Biology*, 287-317.

Ling, T., Lewellen, T., & Miyaoka, R. (2007). Depth of interaction decoding of a continuous crystal detector Module. *Physics in Mediicine and Biology*, 2213-2228.

Pani, R., Pellegrini, R., Cinit, M., Mattioli, M., Trotta, C., Montani, L., et al. (2004). Recent advances and future perspectives of position sensitive PMT. *Nuclear Instruments and Methods in Physics Research B*, 197-205.

Peng, H., & Levin, C. S. (2010, November). Recent Developments in PET Instrumentation. *Current Pharmaceutical Biotechnology*, 555-571.

Peng, H., Olcott, P. D., Pratx, G., Foudray, A. M., Chinn, G., & Levin, C. S. (2007). Design study of a high-resolution breast-dedicated PET. *IEEE Nuclear Science Symposium Conference Record* (pp. 3700-3704). IEEE.

Phelps, M. E., Cherry, S. R., & Dahlbom, M. (2006). *PET - Physics, Instrumentation, ans Scanners.* USA: Springer.

Popov, V. (2011). Advanced data readout technique for Multianode Position Sensitive Photomultiplier Tube applicable in radiation imaging detectors. *12th International Workshop On Radiation Imaging Detectors.* Cambridge.

SPADnet project. (2010, July 1.). Retrieved October 18., 2013, from http://www.spadnet.eu/

Steinbach, C. (2011, October 16.). *Pozitronemissziós tomográf detektormoduljának fejlesztése.* Retrieved October 15., 2013, from BME Kutatói pályázat: http://doktori.bme.hu/bme_palyazat/2011/hallgato/Ocsovaine_Steinbach_Cecilia_hu.htm

Storn, R. (n.d.). *Differential Evolution (DE)*. Retrieved 10 10, 2014, from http://www1.icsi.berkeley.edu/~storn/code.html

Sudhaa , J., Hanumantharajub, M., & Venkateswarulua, V. (2012). A Novel Method for Computing Exponential Function Using CORDIC Algorithm. *International Conference on Communication Technology and System Design 2011*, (pp. 519–528).

Tarantola, G., Zito, F., & Gerundini, P. (2002, October 31). PET Instrumentation and Reconstruction Algorithms in Whole-Body Applications. *Journal of Nuclear Medicine Technology*.

Tropea, S. (2007). FPGA Implementation of Base-N Logarithm. *3rd Southern Conference on Programmable Logic*, (pp. 27 - 32).

Trotta, C., Massari, R., Palermo, N., Scopinaro, F., & Soluri, A. (2007). New high spatial resolution portable camera in medical imaging. *Nuclear Instruments and Methods in Physics Research A*, 604–610.

Trotta, C., Massari, R., Trinci, G., Palermo, N., Boccalini, S., Scopinaro, F., et al. (2008). High-Resolution Imaging System (HiRIS) based on H9500 PSPMT. *Nuclear Instruments and Methods in Physics Research A*, 454-458.

Truman, A., Bird, A., Ramsden, D., & He, Z. (1994). Pixellated COTO arrays with position-sensitive PMT readout. *Nuclear Instruments and Methods in Physics Research A*, 375-378.

van Dam, H., Seifert, S., Vinke, R., Dendooven, P., Löhner, H., Beekman, F., et al. (2011, October). Improved Nearest Neighbor Methods for Gamma Photon Interaction Position Determination in Monolithic Scintillator PET Detectors. *IEEE Transactions on Nuclear Science*, 2139 - 2147.

Walker, R. J., H. C. Braga, L., Erdogan, A. T., Gasparini, L., Grant, L. A., Henderson, R. K., et al. (2013, June). A 92k SPAD Time-Resolved Sensor in 0.13µm CIS Technology for PET/MRI Application. Utah, USA: International Image Sensor Workshop.

Wikipedia: Photomultiplier. (n.d.). Retrieved 10 16, 2014, from http://en.wikipedia.org/wiki/Photomultiplier

Wikipedia: Positron emission tomography. (n.d.). Retrieved 10 15, 2014, from http://en.wikipedia.org/wiki/Positron_emission_tomography

Yuan, W., & Xu, Z. (2013). FPGA based implementation of low-latency floating-point exponential function. *IET International Conference on Smart and Sustainable City 2013*, (pp. 226 - 229).